OPEN ACCESS
IOP Publishing | ISECAEP
Journal of Reliability Science and Engineering
J. Reliab. Sci. Eng. **1** (2025) 015002 (30pp)
https://doi.org/10.1088/3050-2454/ada036

Adaptive artificial neural network for uncertainty propagation

Yan Shi[1,*], Lizhi Niu[2] and Michael Beer[1,3,4]

[1] Institute for Risk and Reliability, Leibniz Universität Hannover, Hannover 30167, Germany
[2] School of Mathematics and Statistics, Northwestern Polytechnical University, Xi'an 710072, People's Republic of China
[3] Department of Civil and Environmental Engineering, University of Liverpool, Liverpool L69 3BX, United Kingdom
[4] International Joint Research Center for Resilient Infrastructure & International Joint Research Center for Engineering Reliability and Stochastic Mechanics, Tongji University, Shanghai 200092, People's Republic of China

E-mail: yan.shi@irz.uni-hannover.de

Received 17 October 2024, revised 24 November 2024
Accepted for publication 9 December 2024
Published 20 January 2025

Abstract

Uncertainty propagation (UP) is a crucial aspect for assessing the influence of input uncertainty on structural responses, holding substantial significance in engineering applications. However, achieving accurate and efficient UP remains challenging, particularly for structures characterized by high nonlinearity and multiple outputs. This study addresses this challenge by proposing a novel adaptive UP method based on the artificial neural network (ANN). In the proposed method, the mean of outputs is analytically derived using the ANN, enabling direct computation of the mean through the weight and bias vectors of the network. An innovative approach is established for solving the standard deviation of outputs, employing several univariate integrals instead of multivariate integrals. The established analytical and univariate integral techniques effectively mitigate post-processing errors commonly encountered when using numerical simulation techniques to estimate the statistical moments of outputs within the ANN context. Furthermore, an adaptive framework is presented, incorporating input space division and an adjustable multi-point addition strategy to enhance computational accuracy in structural UP. Various applications, including highly nonlinear scenarios, multiple outputs, and cases involving finite element models, are presented to demonstrate the effectiveness of the proposed method. The results indicate that the proposed method not only provides accurate estimations of statistical moments but also offers effective estimations of the probability density function of structural outputs.

Keywords: uncertainty propagation, artificial neural network, analytical results, univariate integral, adaptive framework

* Author to whom any correspondence should be addressed.

1. Introduction

Engineering structures invariably exhibit multiple sources of uncertainty, encompassing geometric variations, material property fluctuations, and load environment unpredictability [1]. These uncertainties typically exert a substantial influence on structural responses, and in some cases, may even lead to structural failures [2, 3]. Hence, it is essential to accurately quantify these uncertainties for examining structural responses. Uncertainty propagation (UP) primarily explores the impact of these uncertainty sources on structural responses, playing a pivotal role in the domain of uncertainty quantification [4]. UP encompasses three primary facets, specifically, the determination of statistical moments for outputs [5, 6], the computation of probability density functions (PDFs) for outputs [7, 8], and the evaluation of the likelihood of a particular outcome, such as the failure probability of structures [9, 10]. In general, the UP of engineering structures necessitates the assessment of intricate simulation models and numerous model iterations, rendering it impractical for obtaining precise results with direct numerical simulation techniques in the case of complex or computationally demanding high-fidelity models. Therefore, the development of advanced methods to tackle the substantial costs associated with UP holds considerable engineering significance and has garnered significant attention from researchers.

Currently, numerous efficient methods have been developed to tackle UP issues. For the determination of statistical moments of outputs, various well-established approaches exist, encompassing simulation-based methods [11–13], numerical integration-based techniques [14–16], and surrogate model-based methodologies [17–20], etc. Among the simulation-based methods, Latin hypercube sampling (LHS) [11], Sobol sequences [12], and Halton series [13] stand out as prominent space-filling sampling techniques for determining the sample locations within the input space and calculating corresponding structural outputs to estimate statistical moments. These space-filling sampling techniques are designed to distribute sample points evenly across the input space, maximizing coverage with a minimal number of samples, thereby facilitating efficient estimation of statistical moments for outputs. Numerical integration-based techniques directly approximate integrals defined as statistical moments of outputs through numerical computations. Widely used numerical integration-based methods include the full factorial numerical integration (FFNI) [14], univariate dimension reduction (UDR) [15], and sparse grid numerical integration (SGNI) [16]. FFNI employs an appropriate quadrature formula, typically expressed as a weighted sum of structural output values at specified input points, to estimate statistical moments. The weights and specified input points are determined by applying Gauss–Hermite, Gauss–Legendre, or Gauss–Laguerre quadrature based on the distribution of uncertain input variables [21]. UDR approximates the structural multivariate function by summing several univariate functions, and statistical moments can be calculated using univariate quadrature formulas for each of these univariate functions. Similar to FFNI, SGNI utilizes quadrature formulas based on the Smolyak algorithm to generate far fewer interpolation nodes, yet still highly effective in calculating statistical moments [22]. Surrogate model-based methodologies employ various surrogate models, such as Kriging [23], Gaussian process [24], support vector machine [25], and polynomial chaos expansion [26], to approximate the implicit structural performance function. By replacing the time-consuming implicit performance function with an explicit expression, the statistical moments can then be estimated with high computational efficiency. For example, in [19], an adaptive learning method was developed to calculate the output mean using Gaussian processes. In [5], an efficient method for estimating both the mean and variance of outputs in an analytical manner was presented, leveraging the Kriging surrogate model. Among these approaches, simulation-based methods can yield highly accurate statistical moments when sufficient samples are available. However, their primary limitation lies in the substantial computational cost, rendering them impractical for many engineering applications. In contrast, numerical integration techniques offer improved computational efficiency over simulation-based methods but may introduce significant errors when applied to complex, highly nonlinear structures. Surrogate model-based methodologies often achieve a balance between computational accuracy and efficiency, nonetheless, their effectiveness depends critically on the development of robust strategies and techniques for constructing surrogate models.

To compute the PDFs of outputs, there are several approaches available. The first method involves sampling-based techniques, such as Monte Carlo simulation [27], importance sampling [28], and line sampling [29]. Achieving accurate PDFs often demands a considerable number of samples and simulations based on the sampling-based techniques. The second approach employs moment-based methods, where high-order moments of outputs are combined with specific distribution families to approximate the PDFs. These high-order moments can be estimated using the aforementioned moment estimation methods. Commonly used distribution families include the Pearson system [30], Johnson system [31], and shifted generalized lognormal distribution [32]. The third method utilizes surrogate model-based techniques to create a global surrogate model of the structural performance function, capable of describing the structural behavior across the entire input space. This model is then integrated with sampling-based methods to obtain the PDFs of outputs [33, 34]. For instance, [35] introduces a surrogate model-based method that parameterizes the structure of deep neural networks, enabling these networks to interpret and reconstruct low-dimensional nonlinear manifolds. This approach is applicable for estimating the statistical characteristics and PDF of high-dimensional structural outputs. In [36], a PDF-based sampling technique is proposed to generate high-quality training samples, enhancing the Bayesian neural network (BNN) training process for computing the mean, variance, and PDF of structural outputs. This methodology has also been adapted for dynamic systems by

integrating an arbitrary stochastic process simulation technique [37]. Additionally, [38] presents a novel gradient-enhanced BNN framework that incorporates gradient information during model training, allowing accurate calculation of the first four moments and PDF of structural outputs. Further details on recent advances in surrogate model-based UP techniques can be found in [39]. In summary, surrogate model-based methods continue to be an active and prominent area of research and are increasingly utilized in engineering applications. It is important to note that both sampling-based and surrogate model-based approaches share the respective strengths and limitations of the statistical moment estimation methods discussed in the previous paragraph. For moment-based methods, the need to estimate higher-order moments using the statistical moment estimation methods means their effectiveness depends not only on the choice of distribution families but also on the underlying moment estimation methods.

To evaluate the likelihood of specific outcomes, such as estimating structural failure probability (commonly referred to as reliability analysis), various methods have been developed, including advanced simulation-based techniques [40, 41], high-order moment-based methods [42, 43], and surrogate model-based approaches [44, 45]. Among advanced simulation-based techniques, methods like importance sampling [41], subset simulation [46], and line sampling [47] are well-known for structural reliability analysis. However, these techniques typically require significant computational resources, limiting their practicality in engineering applications. High-order moment-based methods [42, 43] estimate structural failure probability by leveraging multiple statistical moments of structural outputs, offering greater computational efficiency compared to simulation-based techniques, though they may produce large errors for highly nonlinear structures. Surrogate model-based approaches, particularly adaptive surrogate models with efficient learning functions, such as the expected feasibility function [48], U learning function [49], H learning function [50], and the folded normal-based expected improvement function [10], have garnered considerable attention for structural reliability analysis. Further details on structural reliability analysis methods can be found in [9, 51, 52].

While the study of UP problems has seen significant attention, there remains a need to devise efficient methods tailored to address the challenges in UP of structures, particularly in cases characterized by high nonlinearity and multiple outputs. Given the proven effectiveness of the artificial neural network (ANN) [53, 54] in handling issues associated with high nonlinearity and multiple outputs problems, this study develops an accurate and efficient method for tackling structural UP problems, specifically for estimating statistical moments and PDFs of outputs, based on the ANN with a single hidden layer and a Rectified Linear Unit (ReLU) activation function. This work introduces three key innovations. First, an analytical derivation of the mean of outputs based on the ANN is provided. This means that once the ANN is properly constructed, one can easily obtain the mean of outputs using the weight and bias vectors directly. Second, the standard deviation of outputs is estimated by using several univariate integrals rather than multivariate integrals. This novel method offers a fresh approach for estimating the standard deviation of outputs based on the ANN. The established analytical and univariate integral techniques can eliminate the issue of post-processing errors that often occur when using numerical simulation techniques to estimate the mean of outputs in the context of the ANN. Third, an effective adaptive framework that includes input space division and an adjustable multi-point addition strategy is proposed. This framework is designed to enhance the computational accuracy of structural UP.

It is important to note that UP based on ANN has also become a prominent topic within the field of computer science [55]. One widely recognized approach for UP in this area is the layer-wise UP method [56]. In layer-wise UP, the statistical moments of a given layer's output are analytically expressed in terms of the uncertainty of the layer's inputs, under specific assumptions. The uncertainty is then propagated through the network, layer by layer, until it reaches the final output [57]. A key feature of this approach is that approximation techniques, such as piece-wise exponential (PIE) [58] or unscented transform (UT) [59], need to be employed to estimate the statistical moments of the outputs at each hidden layer after applying a nonlinear activation function. However, for very deep and wide ANNs, propagating uncertainty through the nonlinear activation functions of the hidden layers using PIE or UT becomes computationally expensive [60]. Moreover, because these approximation techniques are integral to the UP process, the statistical moments derived from the layer-wise UP approach are inherently approximations rather than exact analytical solutions. In contrast, although the method proposed in this study considers an ANN architecture with a single hidden layer and a ReLU activation function, the analytical and univariate integral techniques are developed to compute the mean and standard deviation of outputs, respectively. The analytical mean of outputs is accurate without introducing approximations during the UP process. Additionally, an adaptive framework that incorporates input space division and an adjustable multi-point addition strategy is introduced, which enhances the computational accuracy of the UP process. This work aims to establish a fresh adaptive approach for UP, and the accuracy and effectiveness of the proposed method are demonstrated in the application section of this paper.

This work is organized as follows. Basic definitions about the UP of structures and ANN are provided in section 2. The novel UP framework is developed in section 3. Several applications regarding UP issues of structures are introduced in section 4. Conclusions are drawn in section 5.

2. Basic definitions

2.1. UP of structures

As the single output problem can be considered a special case of the multiple outputs problem, our attention is directed towards structures with multiple outputs. For a structure with m outputs, the structural performance function can be expressed as $Y_j = g_j(\boldsymbol{X})$ for the jth output, in which

$\boldsymbol{X} = [X_1, X_2, \ldots, X_n]^{\mathrm{T}}$ is n-dimensional random input variables. The marginal PDF of $X_i\,(i = 1, 2, \ldots, n)$ is denoted as $f_{X_i}(X_i)\,(i = 1, 2, \ldots, n)$. The random input variables are supposed to be mutually independent. For the situation where the inputs are dependent, the Rosenblatt transformation [61] can be employed to convert the dependent inputs into independent ones. The joint PDF of the mutually independent random input variables is expressed as $f_X(\boldsymbol{X}) = \prod_{i=1}^{n} f_{X_i}(X_i)$. The mean and standard deviation of outputs possess important role in assess the structural uncertainty, which are defined as follows:

$$\mu_{Y_j} = E(Y_j) = \int_{-\infty}^{+\infty} g_j(\boldsymbol{X}) f_X(\boldsymbol{X})\,\mathrm{d}\boldsymbol{X} \tag{1}$$

$$\sigma_{Y_j} = \sqrt{V(Y_j)} = \sqrt{\int_{-\infty}^{+\infty} \left[g_j(\boldsymbol{X}) - \mu_{Y_j}\right]^2 f_X(\boldsymbol{X})\,\mathrm{d}\boldsymbol{X}} \tag{2}$$

where $E(\cdot)$ and $V(\cdot)$ are expectation and variance operators, respectively. μ_{Y_j} and σ_{Y_j} represent the mean and standard deviation of the jth output, respectively.

Both the above equations involve multivariate integrals, posing a challenge for direct solutions. A classical approach to address these integrals is by employing simulation-based methods [11–13], as outlined below:

$$\mu_{Y_j} = \frac{1}{N}\sum_{k=1}^{N} g_j\left(\boldsymbol{x}^{(k)}\right) \tag{3}$$

$$\sigma_{Y_j} = \sqrt{\frac{1}{N}\sum_{k=1}^{N}\left[g_j\left(\boldsymbol{x}^{(k)}\right) - \mu_{Y_j}\right]^2} \tag{4}$$

in which $\boldsymbol{x}^{(k)} = \left[x_1^{(k)}, x_2^{(k)}, \ldots, x_n^{(k)}\right]^{\mathrm{T}}\,(k = 1, 2, \ldots, N)$ represents the kth sample of random inputs. A significant drawback of simulation-based methods is their challenge in achieving a well-balanced trade-off between computational accuracy and efficiency. This implies that accurate estimation solutions necessitate large samples, a requirement that becomes financially impractical for real engineering structures with intricate finite element models.

2.2. ANN

The ANN is a computational model inspired by the structure and functioning of the human brain. Comprising interconnected nodes, or artificial neurons, organized into layers, the ANN excels at learning complex patterns and relationships from data. Information is processed through the network via weighted connections, and through a process known as training, the network adjusts these weights to optimize its performance on a specific task. The ANN finds applications in a wide range of fields, including image and speech recognition, natural language processing, and pattern classification, making it a powerful tool for solving diverse and complex problems in artificial intelligence. One approach to leverage the ANN in aiding structural UP involves constructing an ANN to approximate the actual performance functions of multiple outputs. Subsequently, simulation-based methods can be integrated to estimate the mean and standard deviation of outputs.

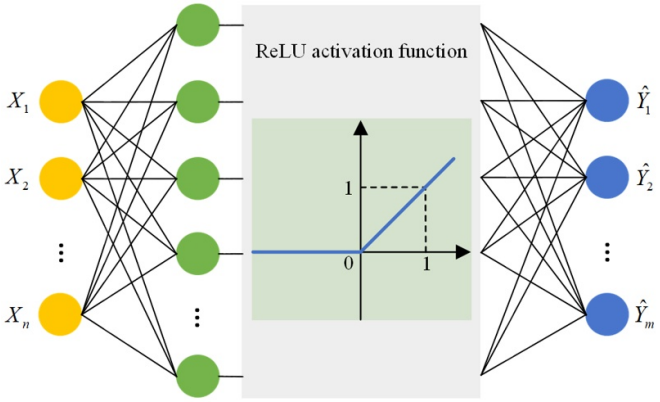

Figure 1. A classic ANN structure.

Activation functions play a crucial role in the functioning of the ANN, serving as non-linear operators that introduce complexity and enable the network to learn intricate patterns. One widely used activation function is the ReLU [62]. ReLU outputs zero for any input that is less than zero and outputs the input itself for positive values. This introduces non-linearity into the model while preserving simplicity, making ReLU particularly useful for complex data representation. One of the main advantages of ReLU is its ability to alleviate the vanishing gradient problem, which can hinder the training of deep networks by slowing down or even halting updates to weights during backpropagation. By ensuring that positive values remain unchanged, ReLU maintains a strong gradient, facilitating faster and more stable learning. Additionally, by setting all negative values to zero, ReLU creates sparsity in the activations, which can lead to improved efficiency and model interpretability. Its computational efficiency and empirical success make ReLU a popular choice in various neural network architectures. Furthermore, the use of the ReLU activation function supports the development of the proposed method, making it a suitable choice for UP problems in this study. It should be noted that only a data-driven model is considered here, while physics-driven models are beyond the scope of this work. A classic ANN structure with single hidden layer and ReLU activation function is shown in figure 1.

In the ANN, the number of artificial neurons in the hidden layer is denoted as n_{H}. Therefore, the responses in the hidden layer can be expressed as follows:

$$Y_{\mathrm{H}} = W^{(1)}X + b^{(1)} \tag{5}$$

where $Y_{\mathrm{H}} = [Y_{\mathrm{H1}}, Y_{\mathrm{H2}}, \ldots, Y_{\mathrm{H}n_{\mathrm{H}}}]^{\mathrm{T}}$. $\boldsymbol{W}^{(1)}$ and $\boldsymbol{b}^{(1)}$ represent the weight and bias vectors between the input and hidden layers, respectively.

$$W^{(1)} = \begin{bmatrix} W_{1,1}^{(1)} & W_{1,2}^{(1)} & \cdots & W_{1,n}^{(1)} \\ W_{2,1}^{(1)} & W_{2,2}^{(1)} & \cdots & W_{2,n}^{(1)} \\ \vdots & \vdots & \ddots & \vdots \\ W_{n_{\mathrm{H}},1}^{(1)} & W_{n_{\mathrm{H}},2}^{(1)} & \cdots & W_{n_{\mathrm{H}},n}^{(1)} \end{bmatrix} \tag{6}$$

$$b^{(1)} = \left[b_1^{(1)}, b_2^{(1)}, .., b_{n_{\mathrm{H}}}^{(1)}\right]^{\mathrm{T}}. \tag{7}$$

Furthermore, the responses after using the ReLU activation function can be expressed as follows:

$$Y_{\mathrm{ReLU}l} = \mathrm{ReLu}\left(Y_{\mathrm{Hl}}\right) = \begin{cases} Y_{\mathrm{Hl}} & Y_{\mathrm{Hl}} \geq 0 \\ 0 & Y_{\mathrm{Hl}} < 0 \end{cases} \tag{8}$$

in which $Y_{\mathrm{Hl}}\,(l = 1, 2, \ldots, n_{\mathrm{H}})$ means the lth response in the hidden layer. $\mathrm{ReLu}\,(\cdot)$ is the ReLU activation function and $Y_{\mathrm{ReLU}} = [Y_{\mathrm{ReLU1}}, Y_{\mathrm{ReLU2}}, \ldots, Y_{\mathrm{ReLU}n_{\mathrm{H}}}]^{\mathrm{T}}$ represents the responses after using the ReLU activation function. The final outputs of the ANN are shown below:

$$\hat{\boldsymbol{Y}} = \boldsymbol{W}^{(2)}\boldsymbol{Y}_{\mathrm{ReLU}} + \boldsymbol{b}^{(2)} \tag{9}$$

where $\hat{\boldsymbol{Y}} = [\hat{Y}_1, \hat{Y}_2, \ldots, \hat{Y}_m]^{\mathrm{T}}$ represents the predicted values of the multiple outputs. $\boldsymbol{W}^{(2)}$ and $\boldsymbol{b}^{(2)}$ represent the weight and bias vectors between the hidden and output layers, respectively.

$$W^{(2)} = \begin{bmatrix} W_{1,1}^{(2)} & W_{1,2}^{(2)} & \cdots & W_{1,n_{\mathrm{H}}}^{(2)} \\ W_{2,1}^{(2)} & W_{2,2}^{(2)} & \cdots & W_{2,n_{\mathrm{H}}}^{(2)} \\ \vdots & \vdots & \ddots & \vdots \\ W_{m,1}^{(2)} & W_{m,2}^{(2)} & \cdots & W_{m,n_{\mathrm{H}}}^{(2)} \end{bmatrix} \tag{10}$$

$$b^{(2)} = \left[b_1^{(2)}, b_2^{(2)}, .., b_m^{(2)}\right]^{\mathrm{T}}. \tag{11}$$

Typically, once the ANN is successfully constructed and trained, simulation-based methods can be incorporated to estimate the mean and standard deviation of outputs. However, this procedure is susceptible to post-processing errors. In the following section, an analytical derivation of the mean of outputs based on the ANN is presented. Additionally, a novel approach is proposed for estimating the standard deviation of outputs, utilizing several univariate integrals instead of multivariate integrals. Furthermore, an adaptive framework is established to enhance the computational accuracy of the ANN.

3. UP framework

Before constructing the novel uncertainty approach, the random input variables $X_i\,(i = 1, 2, \ldots, n)$ are first transformed into standard normal variables $U_i\,(i = 1, 2, \ldots, n)$, using the following equivalent probability transformation technique:

$$U_i = \Phi^{-1}\left(F_{X_i}\left(X_i\right)\right) \tag{12}$$

in which $F_{X_i}(\cdot)$ represents the cumulative distribution function (CDF) of the ith random input variable X_i, and $\Phi^{-1}(\cdot)$ means the inverse CDF of standard normal variables. When constructing the ANN, the training samples are first generated in the standard normal space and transformed into the original probability space, and the corresponding values of outputs are estimated with the multiple real performance functions. Then the training samples in the standard normal space and the corresponding values of outputs in the original probability space are employed to construct the ANN in this work. Therefore, the outputs of the constructed ANN are the outputs (in the original probability space) for the original input variables, and there is no further required transformation. Denote the transformed standard normal variable vector as $\boldsymbol{U} = [U_1, U_2, \ldots, U_n]^{\mathrm{T}}$, then the responses in the hidden layer shown in equation (5) can be rewritten as follows:

$$Y_{\mathrm{H}} = W^{(1)}U + b^{(1)}. \tag{13}$$

In the following subsections, novel approaches for estimating the mean and standard deviation of outputs as well as an adaptive framework are established to accomplish efficient structural UP.

3.1. Mean of outputs

According to the responses in the hidden layer shown in equation (13), the lth response in the hidden layer can be expressed as follows:

$$Y_{\mathrm{Hl}} = \sum_{i=1}^{n} W_{l,i}^{(1)}U_i + b_l^{(1)}. \tag{14}$$

Because $U_i\,(i = 1, 2, \ldots, n)$ are mutually independent standard normal variables, the variable Y_{Hl} is a normal variable with the following mean $\mu_{Y_{\mathrm{Hl}}}$ and standard deviation $\sigma_{Y_{\mathrm{Hl}}}$:

$$\mu_{Y_{\mathrm{Hl}}} = E\left(Y_{\mathrm{Hl}}\right) = \sum_{i=1}^{n} W_{l,i}^{(1)}E\left(U_i\right) + b_l^{(1)} = b_l^{(1)} \tag{15}$$

$$\sigma_{Y_{\mathrm{Hl}}} = \sqrt{V\left(Y_{\mathrm{Hl}}\right)} = \sqrt{\sum_{i=1}^{n} W_{l,i}^{(1)2}V\left(U_i\right)} = \sqrt{\sum_{i=1}^{n} W_{l,i}^{(1)2}}. \tag{16}$$

Utilizing the ReLU activation function described in equation (8), the response $Y_{\mathrm{ReLU}l}\,(l = 1, 2, \ldots, n_H)$ can be further obtained. The propagation of the PDF based on the ReLU activation function is illustrated in figure 2. It is easy to know that the response $Y_{\mathrm{ReLU}l}$ is a censored normal random variable with the following PDF $f_{Y_{\mathrm{ReLU}l}}\left(Y_{\mathrm{ReLU}l}\right)$:

$$f_{Y_{\mathrm{ReLU}l}}\left(Y_{\mathrm{ReLU}l}\right) = \begin{cases} \frac{1}{\sqrt{2\pi}\sigma_{Y_{\mathrm{Hl}}}} \exp\left\{-\frac{\left(Y_{\mathrm{ReLU}l} - \mu_{Y_{\mathrm{Hl}}}\right)^2}{2\sigma_{Y_{\mathrm{Hl}}}^2}\right\} & Y_{\mathrm{ReLU}l} > 0 \\ \Phi\left(-\frac{\mu_{Y_{\mathrm{Hl}}}}{\sigma_{Y_{\mathrm{Hl}}}}\right) & Y_{\mathrm{ReLU}l} = 0 \end{cases} \tag{17}$$

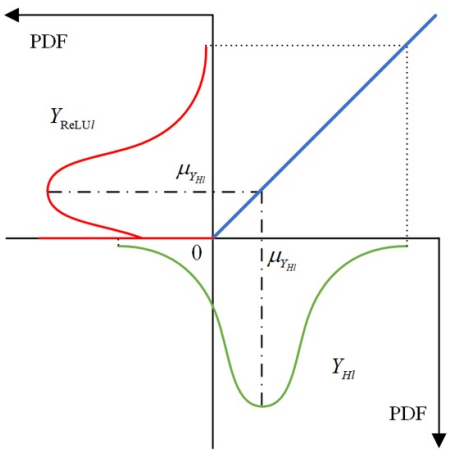

Figure 2. The propagation of PDF based on the ReLU activation function.

in which $\Phi(\cdot)$ means the CDF of standard normal variables. Notably, the reason the PDF becomes $\Phi\left(-\frac{\mu_{Y_{\mathrm{Hl}}}}{\sigma_{Y_{\mathrm{Hl}}}}\right)$ when $Y_{\mathrm{ReLU}l}=0$ is that applying the ReLU activation function converts all values of Y_{Hl} corresponding to $Y_{\mathrm{Hl}}\leqslant 0$ into zero-valued data. Consequently, the sum of PDFs for $Y_{\mathrm{Hl}}\leqslant 0$ aligns with the PDF of $Y_{\mathrm{ReLU}l}=0$, resulting in the PDF of $Y_{\mathrm{ReLU}l}=0$ being equal to $\int_{-\infty}^{0}\frac{1}{\sqrt{2\pi}\sigma_{Y_{\mathrm{Hl}}}}\exp\left\{-\frac{\left(Y_{\mathrm{Hl}}-\mu_{Y_{\mathrm{Hl}}}\right)^2}{2\sigma_{Y_{\mathrm{Hl}}}^2}\right\}\mathrm{d}Y_{\mathrm{Hl}}=\Phi\left(-\frac{\mu_{Y_{\mathrm{Hl}}}}{\sigma_{Y_{\mathrm{Hl}}}}\right)$.

The mean of the response $Y_{\mathrm{ReLU}l}$ can be calculated by:

$$\begin{aligned}\mu_{Y_{\mathrm{ReLU}l}}&=E\left(Y_{\mathrm{ReLU}l}\right)\\&=\int_{0}^{+\infty}Y_{\mathrm{ReLU}l}\frac{1}{\sqrt{2\pi}\sigma_{Y_{\mathrm{Hl}}}}\exp\left\{-\frac{\left(Y_{\mathrm{ReLU}l}-\mu_{Y_{\mathrm{Hl}}}\right)^2}{2\sigma_{Y_{\mathrm{Hl}}}^2}\right\}\mathrm{d}Y_{\mathrm{ReLU}l}\\&\quad+0\times\Phi\left(-\frac{\mu_{Y_{\mathrm{Hl}}}}{\sigma_{Y_{\mathrm{Hl}}}}\right).\end{aligned}\tag{18}$$

The aforementioned integral is analytically derived in this study, and the specific details of this derivation are provided in appendix A. The resulting analytical solution is presented below:

$$\mu_{Y_{\mathrm{ReLU}l}}=\mu_{Y_{\mathrm{Hl}}}\left[1-\Phi\left(-\frac{\mu_{Y_{\mathrm{Hl}}}}{\sigma_{Y_{\mathrm{Hl}}}}\right)\right]+\sigma_{Y_{\mathrm{Hl}}}\phi\left(-\frac{\mu_{Y_{\mathrm{Hl}}}}{\sigma_{Y_{\mathrm{Hl}}}}\right)\tag{19}$$

in which $\phi(\cdot)$ represents the PDF of standard normal variables.

Moreover, according to the predicted values of the multiple outputs shown in equation (9), the predicted values of the jth output can be expressed as follows:

$$\hat{Y}_j=\sum_{l=1}^{n_{\mathrm{H}}}W_{j,l}^{(2)}Y_{\mathrm{ReLU}l}+b_j^{(2)}.\tag{20}$$

Therefore, the mean of the jth output $\hat{Y}_j$ can be obtained by:

$$\begin{aligned}\mu_{\hat{Y}_j}&=E\left(\hat{Y}_j\right)=\sum_{l=1}^{n_{\mathrm{H}}}W_{j,l}^{(2)}E\left(Y_{\mathrm{ReLU}l}\right)+b_j^{(2)}\\&=\sum_{l=1}^{n_{\mathrm{H}}}W_{j,l}^{(2)}\mu_{Y_{\mathrm{ReLU}l}}+b_j^{(2)}.\end{aligned}\tag{21}$$

By combining equations (15), (16), (19) and (21), the analytical solution of mean of the jth output $\hat{Y}_j$ can be derived as follows:

$$\begin{aligned}\mu_{\hat{Y}_j}=\sum_{l=1}^{n_{\mathrm{H}}}W_{j,l}^{(2)}\Bigg\{b_l^{(1)}\left[1-\Phi\left(-\frac{b_l^{(1)}}{\sqrt{\sum_{i=1}^{n}W_{l,i}^{(1)2}}}\right)\right]\\+\sqrt{\sum_{i=1}^{n}W_{l,i}^{(1)2}}\phi\left(-\frac{b_l^{(1)}}{\sqrt{\sum_{i=1}^{n}W_{l,i}^{(1)2}}}\right)\Bigg\}+b_j^{(2)}.\end{aligned}\tag{22}$$

It is evident from equation (22) that the mean of the jth output $\hat{Y}_j$ is computed directly using the weight and bias vectors of the ANN without relying on any simulation techniques. This approach helps circumvent post-processing errors and offers a straightforward way for mean estimation.

3.2. Standard deviation of outputs

In order to estimate the standard deviation of the jth output $\hat{Y}_j$, the standard deviation of response $Y_{\mathrm{ReLU}l}$ is first calculated as follows:

$$\begin{aligned}\sigma_{Y_{\mathrm{ReLU}l}}&=\sqrt{V\left(Y_{\mathrm{ReLU}l}\right)}=\sqrt{E\left(Y_{\mathrm{ReLU}l}^2\right)-E^2\left(Y_{\mathrm{ReLU}l}\right)}\\&=\sqrt{\int_{0}^{+\infty}Y_{\mathrm{ReLU}l}^2\frac{1}{\sqrt{2\pi}\sigma_{Y_{\mathrm{Hl}}}}\exp\left\{-\frac{\left(Y_{\mathrm{ReLU}l}-\mu_{Y_{\mathrm{Hl}}}\right)^2}{2\sigma_{Y_{\mathrm{Hl}}}^2}\right\}\mathrm{d}Y_{\mathrm{ReLU}l}-\mu_{Y_{\mathrm{ReLU}l}}^2}.\end{aligned}\tag{23}$$

We derived the analytical solution of the above integral, and the specific details of this derivation are provided in appendix B.

$$\sigma_{Y_{\mathrm{ReLU}l}}=\sqrt{\mu_{Y_{\mathrm{Hl}}}\sigma_{Y_{\mathrm{Hl}}}\phi\left(-\frac{\mu_{Y_{\mathrm{Hl}}}}{\sigma_{Y_{\mathrm{Hl}}}}\right)+\sigma_{Y_{\mathrm{Hl}}}^{2}+\left(\mu_{Y_{\mathrm{Hl}}}^{2}-\sigma_{Y_{\mathrm{Hl}}}^{2}\right)\Phi\left(-\frac{\mu_{Y_{\mathrm{Hl}}}}{\sigma_{Y_{\mathrm{Hl}}}}\right)-\left[\mu_{Y_{\mathrm{Hl}}}\Phi\left(-\frac{\mu_{Y_{\mathrm{Hl}}}}{\sigma_{Y_{\mathrm{Hl}}}}\right)-\sigma_{Y_{\mathrm{Hl}}}\phi\left(-\frac{\mu_{Y_{\mathrm{Hl}}}}{\sigma_{Y_{\mathrm{Hl}}}}\right)\right]^{2}}. \tag{24}$$

By substituting equations (15) and (16) into above equation, the standard deviation of response $Y_{\mathrm{ReLU}l}$ is obtained as follows:

$$\sigma_{Y_{\mathrm{ReLU}l}}=\sqrt{\begin{aligned}&b_l^{(1)}\sqrt{\sum_{i=1}^{n}W_{l,i}^{(1)2}}\phi\left(-\frac{b_l^{(1)}}{\sqrt{\sum_{i=1}^{n}W_{l,i}^{(1)2}}}\right)+\sum_{i=1}^{n}W_{l,i}^{(1)2}+\left(b_l^{(1)2}-\sum_{i=1}^{n}W_{l,i}^{(1)2}\right)\Phi\left(-\frac{b_l^{(1)}}{\sqrt{\sum_{i=1}^{n}W_{l,i}^{(1)2}}}\right)\\&-\left[b_l^{(1)}\Phi\left(-\frac{b_l^{(1)}}{\sqrt{\sum_{i=1}^{n}W_{l,i}^{(1)2}}}\right)-\sqrt{\sum_{i=1}^{n}W_{l,i}^{(1)2}}\phi\left(-\frac{b_l^{(1)}}{\sqrt{\sum_{i=1}^{n}W_{l,i}^{(1)2}}}\right)\right]^{2}\end{aligned}}. \tag{25}$$

Then, based on the predicted values of the *j*th output shown in equation (20), the standard deviation of the *j*th output can be calculated by:

$$\sigma_{\hat{Y}_j}=\sqrt{V\left(\hat{Y}_j\right)}=\sqrt{V\left(\sum_{l=1}^{n_{\mathrm{H}}}W_{j,l}^{(2)}Y_{\mathrm{ReLU}l}+b_j^{(2)}\right)}=\sqrt{\sum_{l=1}^{n_{\mathrm{H}}}W_{j,l}^{(2)2}\sigma_{Y_{\mathrm{ReLU}l}}^{2}+\sum_{\substack{1\leqslant l_1,l_2\leqslant n_{\mathrm{H}}\\ l_1\neq l_2}}W_{j,l_1}^{(2)}W_{j,l_2}^{(2)}\mathrm{Cov}\left(Y_{\mathrm{ReLU}l_1},Y_{\mathrm{ReLU}l_2}\right)}. \tag{26}$$

in which $\mathrm{Cov}(\cdot,\cdot)$ represents covariance function operator. $\mathrm{Cov}\left(Y_{\mathrm{ReLU}l_1},Y_{\mathrm{ReLU}l_2}\right)$ is further computed with the following transformation.

$$\begin{aligned}&\mathrm{Cov}\left(Y_{\mathrm{ReLU}l_1},Y_{\mathrm{ReLU}l_2}\right)\\&\quad=E\left(Y_{\mathrm{ReLU}l_1}Y_{\mathrm{ReLU}l_2}\right)-E\left(Y_{\mathrm{ReLU}l_1}\right)E\left(Y_{\mathrm{ReLU}l_2}\right)\\&\quad=E\left(Y_{\mathrm{ReLU}l_1}Y_{\mathrm{ReLU}l_2}\right)-\mu_{Y_{\mathrm{ReLU}l_1}}\mu_{Y_{\mathrm{ReLU}l_2}}.\end{aligned} \tag{27}$$

Because both variables $Y_{\mathrm{ReLU}l_1}$ and $Y_{\mathrm{ReLU}l_2}$ are censored normal random variables with the marginal PDF shown in equation (17), thus the expectation for the product of the two variables can be expressed as follows:

$$\begin{aligned}&E\left(Y_{\mathrm{ReLU}l_1}Y_{\mathrm{ReLU}l_2}\right)\\&\quad=\int_0^{+\infty}\int_0^{+\infty}Y_{\mathrm{ReLU}l_1}Y_{\mathrm{ReLU}l_2}f_{Y_{\mathrm{ReLU}l_1}Y_{\mathrm{ReLU}l_2}}\\&\qquad\times\left(Y_{\mathrm{ReLU}l_1},Y_{\mathrm{ReLU}l_2}\right)\mathrm{d}Y_{\mathrm{ReLU}l_1}\mathrm{d}Y_{\mathrm{ReLU}l_2}\end{aligned} \tag{28}$$

where $f_{Y_{\mathrm{ReLU}l_1}Y_{\mathrm{ReLU}l_2}}\left(Y_{\mathrm{ReLU}l_1},Y_{\mathrm{ReLU}l_2}\right)$ is the joint PDF of variables $Y_{\mathrm{ReLU}l_1}$ and $Y_{\mathrm{ReLU}l_2}$ in the positive values domain. In the positive values domain, both variables have normal PDFs shown in equation (17). Therefore, $f_{Y_{\mathrm{ReLU}l_1}Y_{\mathrm{ReLU}l_2}}\left(Y_{\mathrm{ReLU}l_1},Y_{\mathrm{ReLU}l_2}\right)$ is the joint normal PDF depicted by:

$$\begin{aligned}&f_{Y_{\mathrm{ReLU}l_1}Y_{\mathrm{ReLU}l_2}}\left(Y_{\mathrm{ReLU}l_1},Y_{\mathrm{ReLU}l_2}\right)\\&\quad=\frac{1}{2\pi\sigma_{Y_{\mathrm{Hl}_1}}\sigma_{Y_{\mathrm{Hl}_2}}\sqrt{1-\rho_{l_1l_2}^{2}}}\\&\qquad\times\exp\left\{-\frac{1}{2\left(1-\rho_{l_1l_2}^{2}\right)}\left[\frac{\left(Y_{\mathrm{ReLU}l_1}-\mu_{Y_{\mathrm{Hl}_1}}\right)^{2}}{\sigma_{Y_{\mathrm{Hl}_1}}^{2}}\right.\right.\\&\qquad\left.-\frac{2\rho_{l_1l_2}\left(Y_{\mathrm{ReLU}l_1}-\mu_{Y_{\mathrm{Hl}_1}}\right)\left(Y_{\mathrm{ReLU}l_2}-\mu_{Y_{\mathrm{Hl}_2}}\right)}{\sigma_{Y_{\mathrm{Hl}_1}}\sigma_{Y_{\mathrm{Hl}_2}}}\right.\\&\qquad\left.\left.+\frac{\left(Y_{\mathrm{ReLU}l_2}-\mu_{Y_{\mathrm{Hl}_2}}\right)^{2}}{\sigma_{Y_{\mathrm{Hl}_2}}^{2}}\right]\right\}\end{aligned} \tag{29}$$

in which $\rho_{l_1l_2}$ is the correlation coefficient of the two variables. Since in the positive values domain, the joint normal PDF of variables $Y_{\mathrm{ReLU}l_1}$ and $Y_{\mathrm{ReLU}l_2}$ are the same with that of variables Y_{Hl_1} and Y_{Hl_2}, thus the correlation coefficient $\rho_{l_1l_2}$ is the

same with the one between variables Y_{Hl_1} and Y_{Hl_2}. $\rho_{l_1 l_2}$ can be calculated as follows:

$$\begin{aligned}\rho_{l_1 l_2} &= \frac{\mathrm{Cov}\left(Y_{\mathrm{Hl}_1}, Y_{\mathrm{Hl}_2}\right)}{\sqrt{V\left(Y_{\mathrm{Hl}_1}\right)}\sqrt{V\left(Y_{\mathrm{Hl}_2}\right)}} \\ &= \frac{\mathrm{Cov}\left(\sum_{i=1}^{n} W_{l_1,i}^{(1)} U_i + b_{l_1}^{(1)}, \sum_{i=1}^{n} W_{l_2,i}^{(1)} U_i + b_{l_2}^{(1)}\right)}{\sigma_{Y_{\mathrm{Hl}_1}} \sigma_{Y_{\mathrm{Hl}_2}}} \\ &= \frac{\sum_{i=1}^{n} W_{l_1,i}^{(1)} W_{l_2,i}^{(1)}}{\sqrt{\sum_{i=1}^{n} W_{l_1,i}^{(1)2}} \sqrt{\sum_{i=1}^{n} W_{l_2,i}^{(1)2}}}. \end{aligned} \tag{30}$$

While the two-dimensional integral presented in equation (28) can be directly computed using numerical integration methods, this approach is both inefficient and less straightforward compared to univariate integration. In light of this, our study undertakes a transformation and derivation of this integral, converting it into a univariate form for more efficient computation. Detailed steps of this derivation are elucidated in appendix C. The resulting univariate integral is expressed below:

$$\begin{aligned} & E\left(Y_{\mathrm{ReLU}l_1} Y_{\mathrm{ReLU}l_2}\right) \\ &= \int_{-\frac{\sqrt{1-\rho_{l_1 l_2}^2}\mu_{Y_{\mathrm{Hl}_2}}}{\sqrt{2}\sigma_{Y_{\mathrm{Hl}_2}}}}^{+\infty} \frac{\frac{\sqrt{2}\sigma_{Y_{\mathrm{Hl}_2}} v}{\sqrt{1-\rho_{l_1 l_2}^2}} + \mu_{Y_{\mathrm{Hl}_2}}}{2\pi\left(1-\rho_{l_1 l_2}^2\right)} \exp\left\{-\frac{v^2}{1-\rho_{l_1 l_2}^2}\right\} \\ &\quad \times \left(\sqrt{2}\sigma_{Y_{\mathrm{Hl}_1}} Q_1 - \sqrt{\pi}\sqrt{1-\rho_{l_1 l_2}^2}\mu_{Y_{\mathrm{Hl}_1}} Q_2\right) \mathrm{d}v \end{aligned} \tag{31}$$

in which the expressions of Q_1 and Q_2 are provided in equations (C-7) and (C-8) in appendix C. In this study, this univariate integral is computed using high-precision floating-point numerical integration algorithms implemented in the Python package mpmath. Upon solving the univariate integral, we obtain the covariance function as presented in equation (27), subsequently allowing us to determine the standard deviation of the jth output as expressed in equation (26). It is important to highlight that the number of times the integral needs to be computed is solely dependent on the number of artificial neurons in the hidden layer. Given the symmetry of $\mathrm{Cov}\left(Y_{\mathrm{ReLU}l_1}, Y_{\mathrm{ReLU}l_2}\right)$ and $\mathrm{Cov}\left(Y_{\mathrm{ReLU}l_1}, Y_{\mathrm{ReLU}l_2}\right)$, the total number of integrals is $\frac{n_{\mathrm{H}}(n_{\mathrm{H}}-1)}{2}$. These outstanding features render the proposed approach highly effective in addressing challenges associated with high-dimensional inputs and outputs.

3.3. Adaptive framework

To enhance the computational accuracy of the ANN in estimating statistical moments, we introduce an adaptive framework in this subsection. Within this framework, the standard normal input sample space undergoes division into multiple sub-spaces. New training samples are discerned through the application of specific learning functions, established for each sub-space based on the PDFs of untraining samples

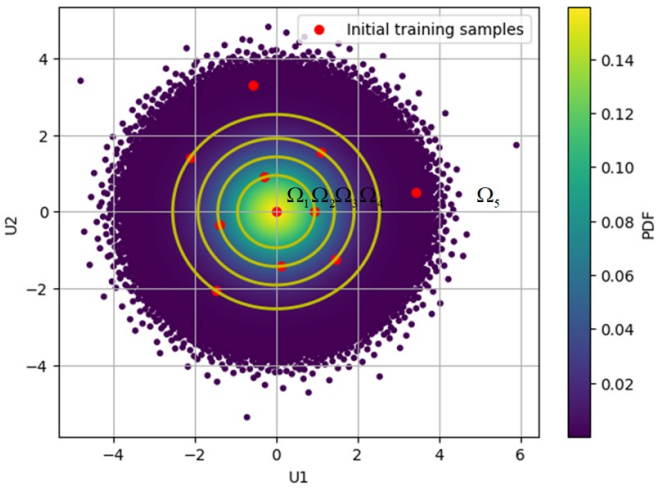

Figure 3. The input space division strategy.

and the distances between training and untraining samples. Furthermore, the quantity of new training samples in each iteration undergoes adaptive adjustment contingent upon the prediction accuracy of the currently constructed ANN in each sub-space. This gives rise to an adaptive framework characterized by input space division and an adjustable multi-point addition strategy.

Regarding the input space division, the process begins by generating N_{Total} total samples using Sobol sequences [12]. These samples are subsequently transformed into the standard normal space through an equivalent probability transformation. Following this, they are reorganized in descending order based on the values of the joint PDF of each sample. It is supposed that the reorganized samples and the corresponding joint PDFs are denoted as $u^{(k)} = [u_1^{(k)}, u_2^{(k)}, \ldots, u_n^{(k)}]^{\mathrm{T}} (k = 1, 2, \ldots, N_{\mathrm{Total}})$ and $\phi_U(u^{(k)}) = \prod_{i=1}^{n} \phi(u_i^{(k)}) (k = 1, 2, \ldots, N_{\mathrm{Total}})$, respectively, in which the smaller the value of the index k, the higher the corresponding joint PDF value. The next step involves dividing the samples into individual sub-spaces sequentially, i.e. $\Omega_1, \Omega_2, \ldots, \Omega_{n_{\mathrm{sub}}}$, with the number of samples in each sub-space being represented by $N_{\mathrm{Total1}}, N_{\mathrm{Total2}}, \ldots, N_{\mathrm{Total}n_{\mathrm{sub}}}$, respectively. The sum of the number of samples in all subspaces is equal to the total number of samples, i.e. $\sum_{s=1}^{n_{\mathrm{sub}}} N_{\mathrm{Totals}} = N_{\mathrm{Total}}$. In this study, n_{sub} is set to 5, and the number of samples in each sub-space is determined by a specified number ratio, i.e. $N_{\mathrm{Total1}} : N_{\mathrm{Total2}} : N_{\mathrm{Total3}} : N_{\mathrm{Total4}} : N_{\mathrm{Total5}} = 9 : 7 : 5 : 3 : 1$. The input space division strategy employed is illustrated in figure 3, where yellow circles depict the boundaries between adjacent sub-spaces.

Once the input space has been effectively partitioned, the initial training samples are identified by selecting the most influential samples within each sub-space based on the N_{Total} total samples. This paper advocates for commencing this process within the first sub-space and subsequently determining training samples in the remaining sub-spaces sequentially. A learning function is formulated to identify the training samples

within each sub-space as follows:

$$u_{\text{News}} = \arg\max \left\{ D_{\min}^{\text{T}}\left(u^{(k)}\right)\left[\phi_U^{\text{T}}\left(u^{(k)}\right)\right]^{\frac{1}{2s-1}} \middle| k = 1 + \sum_{p=1}^{s-1} N_{\text{Total}p}, 2 + \sum_{p=1}^{s-1} N_{\text{Total}p}, \ldots, \sum_{p=1}^{s} N_{\text{Total}p} \right\}. \quad (32)$$

In which $D_{\min}^{\text{T}}\left(\boldsymbol{u}^{(k)}\right)$ represents the normalized minimum Euclidean distance between the current training samples and the kth total sample, and $\phi_U^{\text{T}}\left(\boldsymbol{u}^{(k)}\right)$ means the normalized joint PDF of the kth total sample.

$$D_{\min}^{\text{T}}\left(\boldsymbol{u}^{(k)}\right) = \frac{D_{\min}\left(\boldsymbol{u}^{(k)}\right) - \min\left\{D_{\min}\left(\boldsymbol{u}^{(k)}\right)\right\}}{\max\left\{D_{\min}\left(\boldsymbol{u}^{(k)}\right)\right\} - \min\left\{D_{\min}\left(\boldsymbol{u}^{(k)}\right)\right\}} \quad (33)$$

$$\phi_U^{\text{T}}\left(\boldsymbol{u}^{(k)}\right) = \frac{\phi_U\left(\boldsymbol{u}^{(k)}\right) - \min\left\{\phi_U\left(\boldsymbol{u}^{(k)}\right)\right\}}{\max\left\{\phi_U\left(\boldsymbol{u}^{(k)}\right)\right\} - \min\left\{\phi_U\left(\boldsymbol{u}^{(k)}\right)\right\}} \quad (34)$$

$$D_{\min}\left(u^{(k)}\right) = \min\left\{\left\|u_{\text{Training}} - u^{(k)}\right\|\right\} \quad (35)$$

where u_{Training} represents all current training samples in sub-spaces, and $\|\cdot\|$ is the 2-norm operator. Utilizing the devised learning function, on one hand, samples with large joint PDFs are more likely to be chosen as new training samples. This preference arises from the significant impact these samples exert on estimating the statistical moments of the outputs. Additionally, introducing an exponential parameter within the density term, which diminishes with the escalation of sub-space indicators, allows for the differentiation of the density influence across various sub-spaces. On the other hand, the Euclidean distance term ensures a uniform arrangement of training samples within the input space to the extent possible. This arrangement contributes to an enhanced overall prediction accuracy of the ANN across the entire input space. Denoting the number of initial training samples in the sth sub-space as N_{Initials}. This work employs the first sample, i.e. $\boldsymbol{u}^{(1)} = \left[u_1^{(1)}, u_2^{(1)}, \ldots, u_n^{(1)}\right]^{\text{T}}$, to be the first training sample. Subsequently, the second training sample is determined using equation (32) within the 1th sub-space. The existing training samples are updated, and the identification process is iterated to obtain the third sample within the 1th sub-space. This procedure continues until the number of training samples in the 1th sub-space reaches the desired quantity, i.e. N_{Initial1}. Following this, the training samples within the 2th sub-space are obtained through a similar iterative process. The acquisition of training samples in the remaining sub-spaces follows the same procedure. Figure 3 shows the initial training samples when $N_{\text{Initial1}} = 3$ and $N_{\text{Initials}} = 2\,(s = 2,3,4,5)$.

Based on the current training samples, i.e. u_{Training}, the corresponding structural outputs can be calculated with the actual performance functions. The ANN of the structural responses can then be constructed. In this work, the mean squared error loss function is employed and the number of artificial neurons in the hidden layer is identified as follows:

$$n_{\text{H}} = \max\{50, 2n\}. \quad (36)$$

The adaptive framework is designed to enhance the prediction accuracy of the ANN by incorporating the most influential samples into the training sample set during each iteration. Consequently, the prediction results derived from the ANN at two consecutive iterations serve as a metric for assessing the convergence status of the adaptive framework. This study employs the subsequent prediction error expression to gauge the prediction accuracy of the ANN for the jth output:

$$\delta_j = \frac{\sum_{k=1}^{N_{\text{Total}}} \left|\hat{Y}_j^q\left(u^{(k)}\right) - \hat{Y}_j^{q-1}\left(u^{(k)}\right)\right|}{\left|\sum_{k=1}^{N_{\text{Total}}} \hat{Y}_j^q\left(u^{(k)}\right)\right|} \quad (37)$$

in which $\hat{Y}_j^{q-1}\left(\boldsymbol{u}^{(k)}\right)$ and $\hat{Y}_j^q\left(\boldsymbol{u}^{(k)}\right)$ represent the predicted values for the jth output at the $(q-1)$th and qth iterations. Simultaneously, the relative errors of predicted statistical moments at two consecutive iterations can be also used to measure the convergence status of the estimation of statistical moments.

$$\lambda_{\mu_j} = \left| \frac{\sum_{k=1}^{N_{\text{Total}}} \hat{Y}_j^q\left(u^{(k)}\right) - \sum_{k=1}^{N_{\text{Total}}} \hat{Y}_j^{q-1}\left(u^{(k)}\right)}{\sum_{k=1}^{N_{\text{Total}}} \hat{Y}_j^q\left(u^{(k)}\right)} \right| \quad (38)$$

$$\lambda_{\sigma_j} = \frac{\sqrt{\frac{1}{N_{\text{Total}}}\sum_{k=1}^{N_{\text{Total}}}\left[\hat{Y}_j^q\left(\boldsymbol{u}^{(k)}\right) - \frac{1}{N_{\text{Total}}}\sum_{k=1}^{N_{\text{Total}}}\hat{Y}_j^q\left(\boldsymbol{u}^{(k)}\right)\right]^2} - \sqrt{\frac{1}{N_{\text{Total}}}\sum_{k=1}^{N_{\text{Total}}}\left[\hat{Y}_j^{q-1}\left(\boldsymbol{u}^{(k)}\right) - \frac{1}{N_{\text{Total}}}\sum_{k=1}^{N_{\text{Total}}}\hat{Y}_j^{q-1}\left(\boldsymbol{u}^{(k)}\right)\right]^2}}{\sqrt{\frac{1}{N_{\text{Total}}}\sum_{k=1}^{N_{\text{Total}}}\left[\hat{Y}_j^q\left(\boldsymbol{u}^{(k)}\right) - \frac{1}{N_{\text{Total}}}\sum_{k=1}^{N_{\text{Total}}}\hat{Y}_j^q\left(\boldsymbol{u}^{(k)}\right)\right]^2}}. \quad (39)$$

058

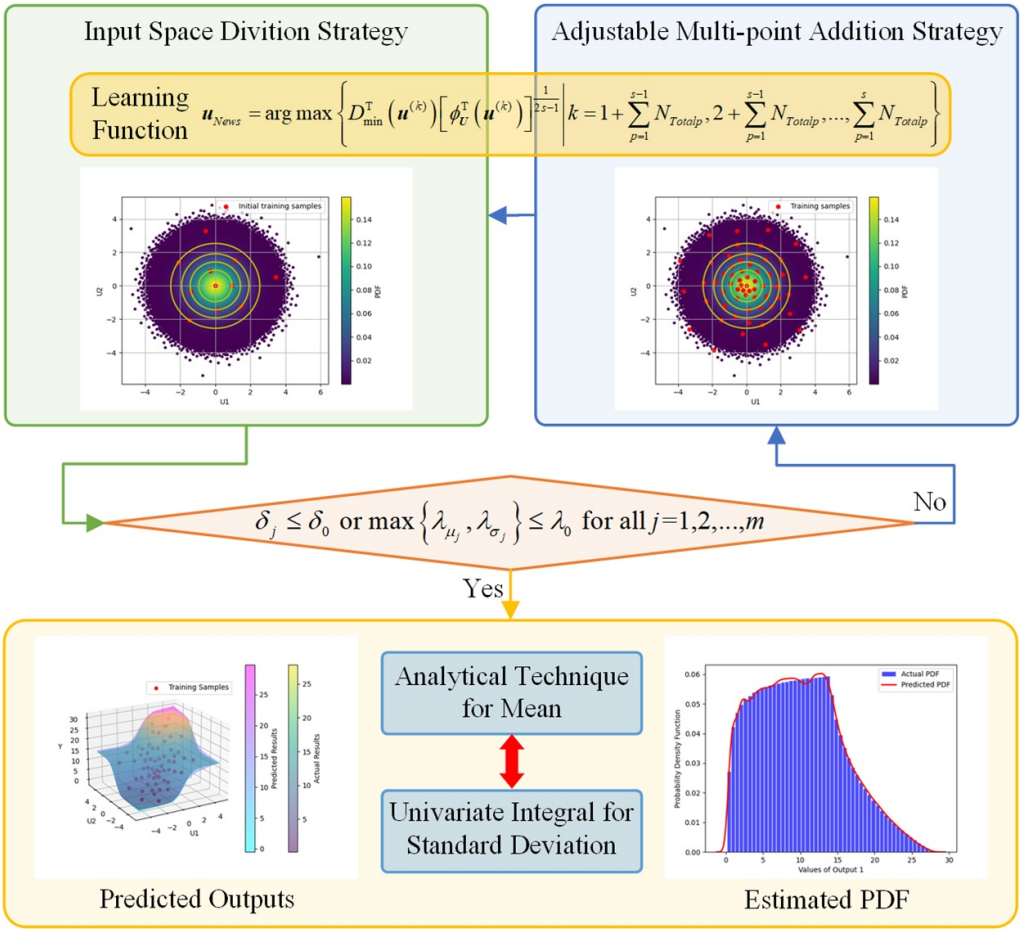

Figure 4. The framework of the proposed adaptive UP approach.

The adaptive updating process is iteratively executed until the following convergence criterion is matched:

$$\delta_j \leqslant \delta_0 \text{ or } \max\left\{\lambda_{\mu_j}, \lambda_{\sigma_j}\right\} \leqslant \lambda_0 \text{ for all } j = 1,2,\ldots,m \quad (40)$$

where δ_0 and λ_0 are convergence thresholds.

If the convergence criterion specified in equation (40) is not met, the subsequent expression is employed to identify the indices of outputs that require updating:

$$j_{\text{Update}} = \arg\text{find}\left\{\delta_j > \delta_0 | j = 1,2,\ldots,m\right\}. \quad (41)$$

For the j_{Update}th output, the errors between the actual and predicted solutions for the current training samples can be calculated by:

$$\text{Error} = \left| g_{j_{\text{Update}}}\left(x_{\text{Training}}\right) - \hat{Y}^{q}_{j_{\text{Update}}}\left(u_{\text{Training}}\right) \right| \quad (42)$$

in which x_{Training} is the training samples in original input space that obtained by u_{Training} through the equivalent probability transformation. We reorganize the current training samples in descending order based on the values of the Error of each sample. The first $2n_{\text{sub}}$ samples are selected as the samples that possess large prediction errors, and the subspaces where these samples are located can be further determined. Subsequently, a new training sample in each determined sub-space is selected based on the established learning function shown in equation (32). The corresponding structural outputs are then calculated with the actual performance functions. The new training samples and structural outputs are added to the training sample set and response set, respectively, to reconstruct the ANN. This forms an adjustable multi-point addition strategy. The updating process is iteratively executed until the convergence criterion shown in equation (40) is matched. Finally, the mean and standard deviation of outputs are computed based on the approach provided in sections 3.1 and 3.2, respectively. It should be noted that the data is standardized when constructing the ANN. The framework of the proposed adaptive UP approach is depicted in figure 4.

4. Applications

Several examples, encompassing highly nonlinear scenarios, multiple outputs, and cases involving finite element models, have been employed to substantiate the efficacy of the proposed method in tackling UP challenges. In this study, the total number of samples for the proposed method is defined

as $N_{\text{Total}} = 2^{20} = 1048576$. As reference methods, we utilize the LHS [11], Sobol sequences [12], Halton series [13], FFNI [14], SGNI [16], convolutional neural network (CNN) [63], and Monte Carlo simulation (MCS). The solutions based on the MCS are regarded as the actual ones. The CNN comprises a single convolutional layer followed by two linear neural networks, each employing the ReLU activation function. In the convolutional layer, the parameters for the convolution kernel, stride, and pooling are configured as 1×2, 1×1, and 0×1, respectively. Additionally, the max-pooling layer is characterized by a convolution kernel size and stride set at 1×2. The CNN is constructed with an equivalent computational cost to that of the proposed method, and the mean and standard deviation are calculated based on equations (3) and (4), respectively. For the proposed method and CNN, the widely used mean squared error loss function and Adam optimization algorithm [64] are employed to identify the optimal weight and bias vectors. The hyper parameter optimization and machine learning models execution are implemented in Python 3.9, on a computer with Intel Core™ i7–7700 CPU at 3.60 GHz and 16 GB RAM. The thresholds of the convergence criterion for all these examples are set to $\delta_0 = 0.005$ and $\lambda_0 = 0.001$.

4.1. Highly nonlinear cases

Considering the following three highly nonlinear structural performance functions:

$$\begin{aligned} \text{Case 1}: g(X) &= \sin(X_1 + 1) + 0.1X_2 \quad X_i\,(i = 1,2) \\ &\sim \text{Uniform}\left(3 - 3\sqrt{3}, 3 + 3\sqrt{3}\right) \end{aligned} \tag{43}$$

$$\begin{aligned} \text{Case 2}: g(X) &= 0.4\cos^3(X_1) + \exp\left\{\sin^2(0.4X_2)\right\} - 1 \\ &\times X_1 \sim \text{Lognormal}(10,1), X_2 \\ &\sim \text{Normal}(10,1) \end{aligned} \tag{44}$$

$$\begin{aligned} \text{Case 3}: g(X) &= \sin(X_1) + 7\sin^2(X_2) + 0.01X_3^4\sin(X_1) \\ &\times X_i\,(i = 1,2,3) \sim \text{Uniform}(-\pi, \pi) \end{aligned} \tag{45}$$

in which the distribution parameters of inputs for normal and lognormal distributions represent the mean and standard deviation, and for uniform distribution represent the lower and upper bounds.

For the three highly nonlinear cases, the proposed method is adaptively executed to estimate the mean and standard deviation results of outputs. Subsequently, the Sobol, Halton, LHS, and CNN methods are employed to compute mean and standard deviation results of outputs, maintaining an equivalent computational cost to that of the proposed method. Additionally, the mean and standard deviation results of outputs using the FFNI, SGNI with a precision level of $q = 8$, and MCS are also presented. In the case of MCS, a substantial number of samples are utilized to ensure accurate estimation results for statistical moments. The obtained mean and standard deviation results for Case 1, Case 2, and Case 3 are summarized in tables 1–3, respectively. Furthermore, the evolutions of statistical moments estimated by the proposed method are depicted in figures 5, 9 and 13, corresponding to Case 1, Case 2, and Case 3, respectively. It is essential to highlight that in figures 5, 9 and 13, the simulated results reflect estimations based on the N_{Total} total samples and actual performance functions, while the predicted results are based on the N_{Total} total samples and the constructed ANN model at each iteration. Upon completion of the adaptive updating process in the proposed method, the analytical and univariate integral techniques established in this work are employed to determine the mean and standard deviation results of outputs. The corresponding results for Case 1, Case 2, and Case 3 are illustrated in figures 6, 10 and 14, respectively. These figures also include simulated results with error bars at different sample sizes based on the constructed ANN model. Furthermore, figures 7 and 11 showcase the training samples and structural responses based on the proposed method for Case 1 and Case 2, respectively. The PDFs of structural outputs for Case 1, Case 2, and Case 3 are presented in figures 8, 12 and 15, respectively.

Table 1. Mean and standard deviation results for Case 1.

Methods	Mean	$\Delta_\mu/\%$	Standard deviation	$\Delta_\sigma/\%$	N_{call}
FFNI	0.0279	93.49	0.7929	5.24	11
SGNI ($q = 8$)	0.6016	40.27	0.6766	10.19	201
Sobol	0.4306	0.40	0.7557	0.31	155
Halton	0.4323	0.78	0.7554	0.27	
LHS	0.4271	0.43	0.7869	4.44	
CNN	0.4259	0.70	0.7435	1.31	
Proposed	0.4291	0.04	0.7517	0.22	
MCS	0.4289	—	0.7534	—	10^8

Note: Δ_μ and Δ_σ represent the relative errors between the MCS and the other methods for the mean and standard deviation, respectively. N_{call} is the computational cost describing the number of calling the actual performance function.

Table 2. Mean and standard deviation results for Case 2.

Methods	Mean	$\Delta_\mu/\%$	Standard deviation	$\Delta_\sigma/\%$	N_{call}
FFNI	0.7159	9.27	0.7019	27.09	11
SGNI ($q = 8$)	0.6571	0.30	0.5558	0.63	201
Sobol	0.6415	2.08	0.5383	2.53	65
Halton	0.6523	0.43	0.5411	2.03	
LHS	0.6581	0.45	0.5700	3.21	
CNN	0.6628	1.16	0.5459	1.14	
Proposed	0.6558	0.10	0.5503	0.38	
MCS	0.6552	—	0.5523	—	10^8

Table 3. Mean and standard deviation results for Case 3.

Methods	Mean	$\Delta_\mu/\%$	Standard deviation	$\Delta_\sigma/\%$	N_{call}
FFNI	0	100	0	100	16
SGNI ($q = 8$)	4.9792	42.26	2.7406	4.54	1233
Sobol	3.5306	0.87	2.6119	0.37	161
Halton	3.4886	0.33	2.6255	0.15	
LHS	3.4991	0.03	2.6783	2.16	
CNN	3.3617	3.95	2.7306	4.16	
Proposed	3.4982	0.05	2.6129	0.33	
MCS	3.5000	—	2.6216	—	10^8

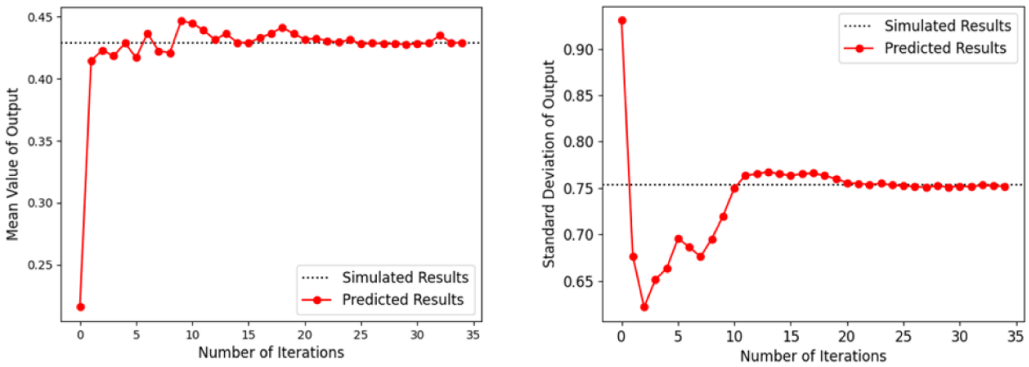

(a) Mean of output (b) Standard deviation of output

Figure 5. Evolution of statistical moments with the number of iterations for Case 1.

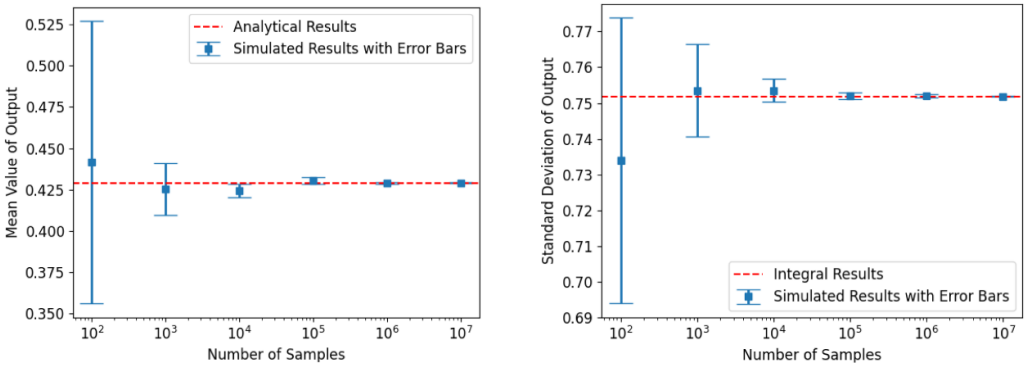

(a) Mean of output (b) Standard deviation of output

Figure 6. Predicted statistical moments for Case 1.

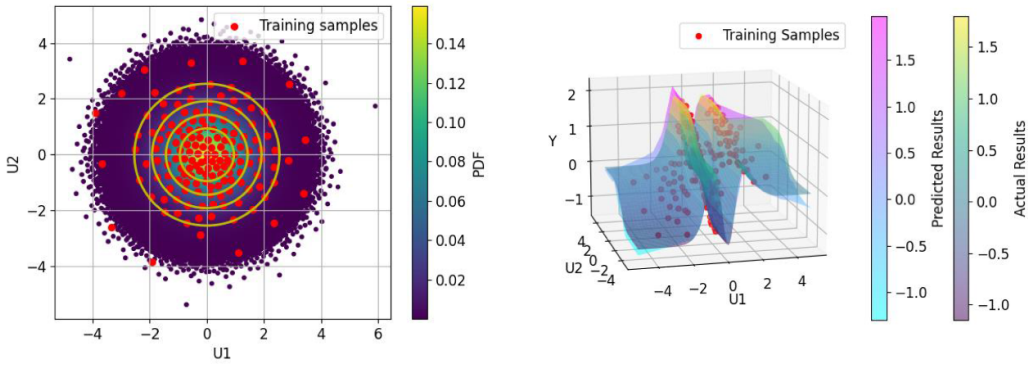

(a) Training samples (b) Structural responses

Figure 7. Training samples and structural responses for Case 1.

The convergence characteristics of the proposed method are evident in figures 5, 9 and 13, where an increase in the number of iterations leads to the gradual convergence of predicted statistical moments towards the corresponding simulated results. This observation underscores the favorable convergence behavior inherent in the proposed method. Furthermore, figures 6, 10 and 14 reveal that the simulated results align closely with the calculated mean, based on the established analytical technique, and the calculated standard deviation, based on the established univariate integral technique, only when a sufficient number of samples are utilized. This observation underscores the effectiveness of the established analytical and univariate integral techniques. It is noteworthy that these techniques play a crucial role in mitigating post-processing errors that may arise when employing numerical simulation techniques to estimate statistical moments of outputs within the framework of the ANN.

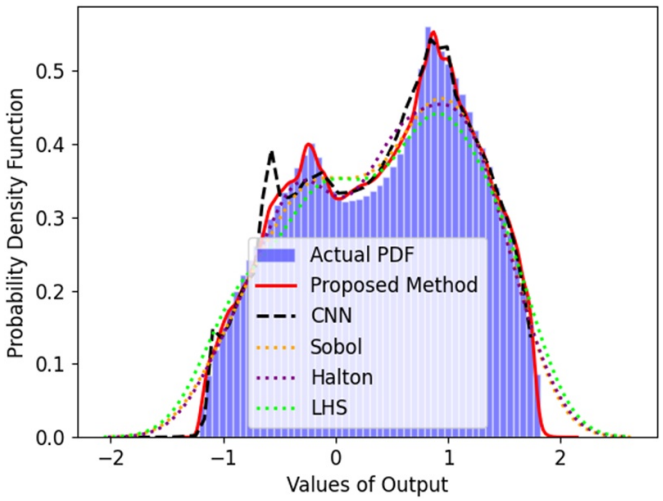

Figure 8. PDF of structural output for Case 1.

The mean and standard deviation results presented in tables 1 and 2 underscore the superior accuracy of the proposed method in estimating statistical moments, with the maximum error being only 0.38%. In contrast, despite FFNI exhibiting the highest efficiency, its accuracy is notably deficient in highly nonlinear cases, registering a substantial maximum error of 93.49%. The other methods exhibit varying degrees of error, for instance, SGNI demonstrates significant error in estimating the mean of output for Case 1, while LHS exhibits considerable error in estimating the standard deviation of output for Case 2. For the mean and standard deviation results detailed in table 3 for Case 3, the proposed method consistently provides accurate estimations, with relative errors of 0.05% and 0.33%, respectively. Although LHS and Halton offer the most accurate estimations for the mean and standard deviation individually, they falter in accurately estimating the standard deviation and mean, respectively, when compared to the corresponding results obtained through the proposed method. Furthermore, FFNI exhibits the largest errors, and SGNI incurs substantial errors along with demanding significant computational costs. These findings underscore the effectiveness of the proposed method in accurately estimating the statistical moments of structural outputs.

Observing figures 7 and 11 reveals that the majority of training samples are strategically concentrated within domains characterized by high PDF and pronounced nonlinearity. This strategic selection enhances the precision of the constructed ANN models in these crucial domains, thereby affirming the effectiveness of the established adaptive framework. Furthermore, the PDFs depicted in figures 8, 12 and 15 underscore that the proposed method excels in accuracy when compared to alternative methods. While CNN yields relatively accurate estimations of PDFs for Case 1 and Case 2, it exhibits substantial errors for Case 3. Moreover, the PDFs estimated by the Sobol, Halton, and LHS methods display significant errors across all three cases. This emphasizes the capability of the proposed method to not only provide accurate estimations of statistical moments but also to deliver effective estimations of the PDFs of structural outputs.

4.2. *Multiple outputs example*

A multiple outputs example [65] is employed to illustrate the effectiveness of the proposed method in dealing with UP problems. This example involves ten outputs, each associated with specific performance functions, as detailed below:

$$\begin{cases} g_1(\boldsymbol{X}) = 1.16 - 0.3717X_2X_4 - 0.00931X_2X_{10} - 0.484X_3X_9 + 0.01343X_6X_{10} - 1 \\ g_2(\boldsymbol{X}) = 4.72 - 0.5X_4 - 0.19X_2X_3 - 0.0122X_4X_{10} + 0.009325X_6X_{10} + 0.000191X_{11}^2 - 4.01 \\ g_3(\boldsymbol{X}) = 29.89 + 3.818X_3 - 4.2X_1X_2 + 0.0207X_5X_{10} + 6.63X_6X_9 - 7.7X_7X_8 + 0.32X_9X_{10} - 32 \\ g_4(\boldsymbol{X}) = 33.86 + 2.95X_3 + 0.1729X_{10} - 5.057X_1X_2 - 11X_2X_8 - 0.0215X_5X_{10} - 9.98X_7X_8 + 22X_8X_9 - 32 \\ g_5(\boldsymbol{X}) = 46.36 - 9.9X_2 - 12.9X_1X_8 + 0.1107X_3X_{10} - 32 \\ g_6(\boldsymbol{X}) = 0.261 - 0.0159X_1X_2 - 0.188X_1X_8 - 0.019X_2X_7 + 0.0144X_3X_5 + 0.0008757X_5X_{10} - 0.32 \\ g_7(\boldsymbol{X}) = 0.214 + 0.00817X_5 - 0.131X_1X_8 - 0.0704X_1X_9 + 0.03099X_2X_6 - 0.018X_2X_7 + 0.0208X_3X_8 \\ \qquad +0.121X_3X_9 - 0.00364X_5X_6 + 0.0007715X_5X_{10} - 0.0005354X_6X_{10} + 0.00121X_8X_{11} - 0.32 \\ g_8(\boldsymbol{X}) = 0.74 - 0.61X_2 - 0.163X_3X_8 + 0.001232X_3X_{10} - 0.166X_7X_9 + 0.227X_2^2 - 0.32 \\ g_9(\boldsymbol{X}) = 10.58 - 0.674X_1X_2 - 1.95X_2X_8 + 0.02054X_3X_{10} - 0.0198X_4X_{10} + 0.0281X_6X_{10} - 9.9 \\ g_{10}(\boldsymbol{X}) = 16.45 - 0.489X_3X_7 - 0.843X_5X_6 + 0.0432X_9X_{10} - 0.0556X_9X_{11} - 0.000786X_{11}^2 - 15.69 \end{cases} \tag{46}$$

in which the distribution parameters of the random variables $X_i\,(i = 1, 2, \ldots, 11)$ are listed in table 4.

For the multiple outputs example, only one ANN model needs to be constructed based on the proposed adaptive framework to predict ten outputs simultaneously. The mean and standard deviation results for these ten outputs, obtained through various methods, are detailed in tables 5–14. Corresponding PDFs are presented in figure 16. The mean and standard deviation results affirm that the proposed method consistently delivers relatively accurate estimations of

062

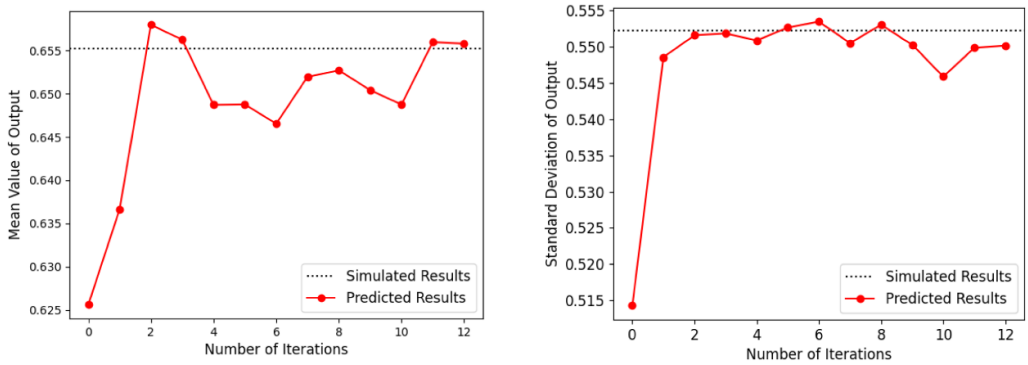

(a) Mean of output (b) Standard deviation of output

Figure 9. Evolution of statistical moments with the number of iterations for Case 2.

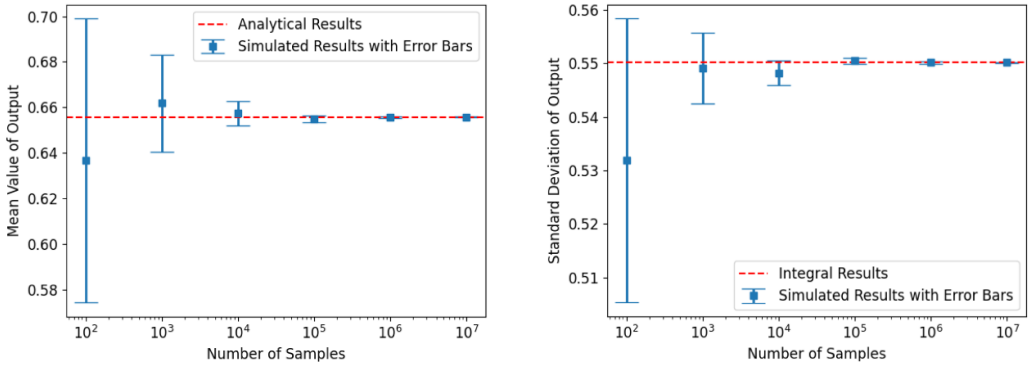

(a) Mean of output (b) Standard deviation of output

Figure 10. Predicted statistical moments for Case 2.

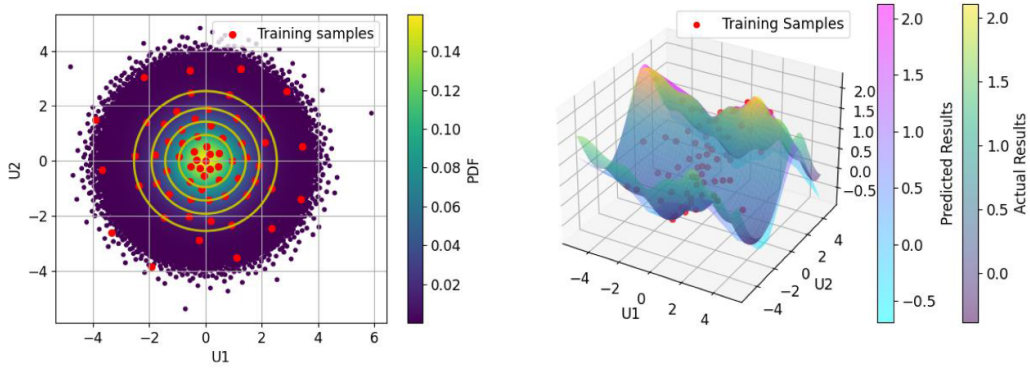

(a) Training samples (b) Structural responses

Figure 11. Training samples and structural responses for Case 2.

statistical moments for all ten outputs. Computational costs for each output are determined within the established adaptive framework, ranging from a minimum of 32 for output 6 to a maximum of 273 for output 2. The aggregate computational costs for the proposed method total 1290. While the SGNI method provides the most accurate estimations of statistical moments for all ten outputs, its total computational costs amount to 2650, which are more than twice those of the proposed method. The FFNI method also offers accurate estimations for some outputs but introduces significant errors for others, such as a 10.67% relative error in the estimation of the standard deviation for output 2. Other methods may yield accurate estimations for certain outputs but exhibit substantial errors for others. The most significant error introduced by the proposed method is in the estimation of the standard deviation for output 7, with a relative error of 8.49%. However, it is important to note that the absolute error for this case is small, given that the actual standard deviation is 0.0049, while the

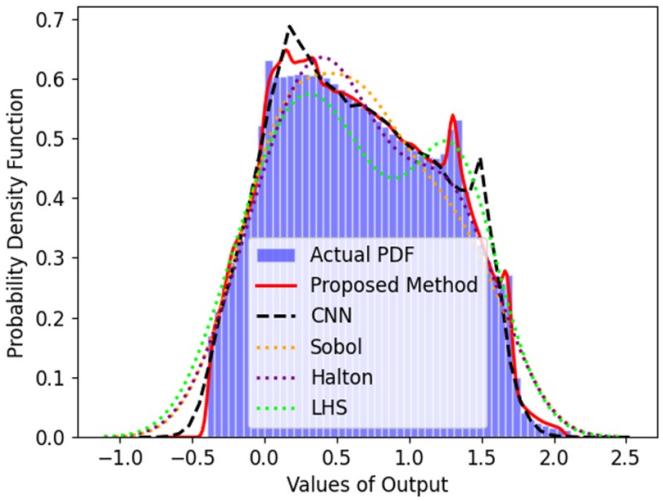

Figure 12. PDF of structural output for Case 2.

predicted value is 0.0045. In summary, the proposed method consistently provides relatively accurate and stable estimations of statistical moments for multiple outputs. Additionally, the PDFs depicted in figure 16 illustrate that the proposed method offers the most accurate estimation of PDFs for all ten outputs comparing with other methods, underscoring its effectiveness in addressing UP in multiple outputs problems.

4.3. A planetary transmission gear

Planetary transmission gears present numerous advantages, encompassing a compact structure, small size, high transmission ratio, and elevated efficiency. Consequently, they find extensive application in various engineering domains, including automobiles, vessels, and geared turbofan engines. Illustrated in figure 17(a), a typical planetary transmission gear [66] comprises one sun gear, three planetary gears, and one gear ring. The gear parameters, including the pressure angle, module, and tooth width, are uniformly set at 20 degrees, 1.5 mm, and 30 mm, respectively. The respective tooth counts for the sun gear, planetary gear, and gear ring are 36, 21, and 78. During operation, the sun gear functions as the input gear, with the planetary gears fixed in the direction of revolution, and the gear ring serving as the output gear. In this study, stress analysis solutions at positions A, B, C, and D, as depicted in figure 17(b), are considered as the multiple outputs of the planetary transmission gear. The corresponding performance functions for the planetary transmission gear are provided below:

$$\begin{cases} g_1(\boldsymbol{X}) = S_A(E, \nu, m, T) \\ g_2(\boldsymbol{X}) = S_B(E, \nu, m, T) \\ g_3(\boldsymbol{X}) = S_C(E, \nu, m, T) \\ g_4(\boldsymbol{X}) = S_D(E, \nu, m, T) \end{cases} \tag{47}$$

in which E, ν, m, and T represent the elastic modulus, Poisson's ratio, friction coefficient, and transmitted torque of the planetary transmission gear, respectively. All these parameters are considered as random variables, and their corresponding distribution parameters are listed in table 15.

For the UP analysis of the planetary transmission gear, we constructed a singular ANN model using the proposed method to simultaneously estimate the statistical moments of its four outputs. The mean and standard deviation results for these four outputs are detailed in tables 16–19. Additionally, the results of statistical moments based on established analytical and univariate integral techniques are illustrated in figure 18. The PDFs for the four outputs are presented in figure 19. In this specific application, the adaptive process of the proposed method was terminated after two iterations, yielding final statistical moments results with a computational cost of 16 for each output. The obtained results highlight the capability of the proposed method to provide relatively accurate estimations of the statistical moments for all four outputs. In contrast, alternative methods may accurately estimate statistical moments for some outputs but exhibit significant errors for others. For instance, the LHS method can accurately estimate the mean for output 2 but introduces a substantial error in estimating the standard deviation of output 2, with a relative error of 10.59%. Figure 18 reveals a close alignment between the simulated results and the calculated mean, derived from the established analytical technique, as well as the calculated standard deviation, derived from the established univariate integral technique, when a sufficient number of samples are employed. This observation underscores the efficacy of both the established analytical and univariate integral techniques. Moreover, the PDFs depicted in figure 19 highlight that the proposed method can provide the most accurate estimations of PDFs for all four outputs, illustrating the effectiveness of the proposed method in addressing the UP of the planetary transmission gear.

4.4. An airplane wing

The UP of the airplane wing [38] is a critical aspect in aeronautical engineering, as it constitutes a fundamental element of the aircraft's structural integrity. Illustrated in figure 20 is a model of an airplane wing with a chord length of 1000 mm, an extension length of 4000 mm, and incorporating main and auxiliary I-beams, 15 long trusses, and 9 wing ribs. The spacing between adjacent wing ribs is set at 500 mm, and a NACA0012 symmetric airfoil is employed in this airplane wing. The wing I-beams are fabricated from 30CrMnSiNi2A alloy steel, while the long trusses, wing ribs, and skin are constructed using 2024 aluminum alloy. During flight, the wings of the airplane are subjected to aerodynamic loads, with figure 21 providing insight into the performance of the airplane wing under these loads. In this study, the stress solution at position A of the skeleton structure depicted in figure 21(a) and the strain solution at position B of the skin structure shown in figure 21(b) are regarded as the multiple outputs of the airplane wing. The respective performance functions for the airplane wing are

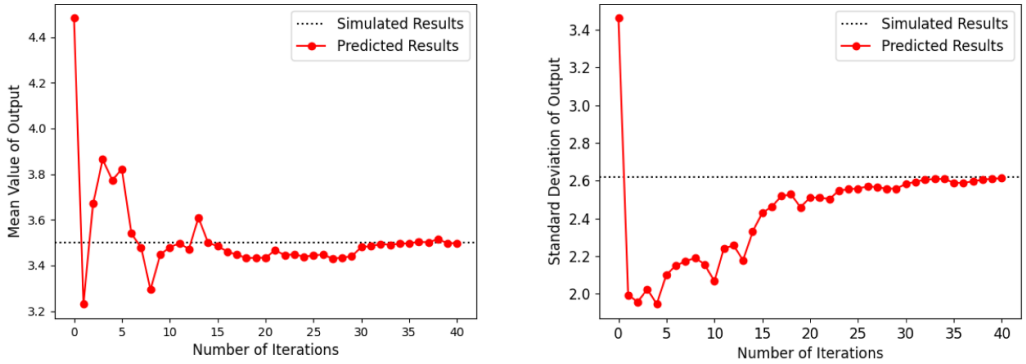

(a) Mean of output (b) Standard deviation of output

Figure 13. Evolution of statistical moments with the number of iterations for Case 3.

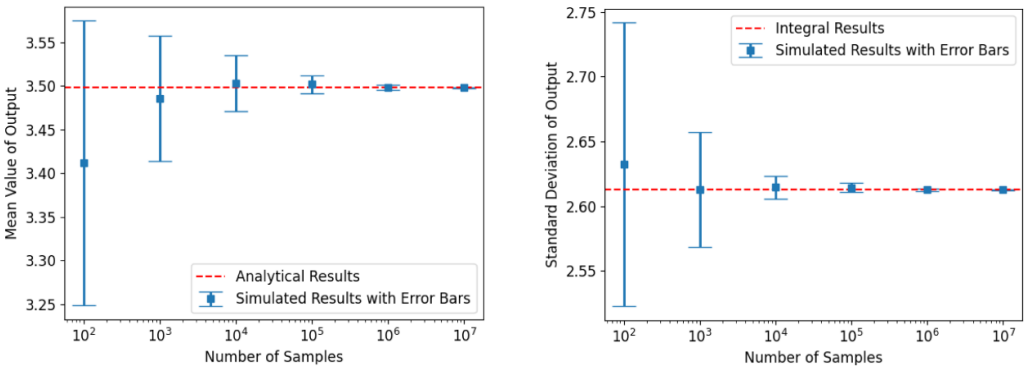

(a) Mean of output (b) Standard deviation of output

Figure 14. Predicted statistical moments for Case 3.

$$\begin{cases} g_1(\boldsymbol{X}) = S_A\left(E_1,\rho_1,\nu_1,E_2,\rho_2,\nu_2,\gamma_{\mathrm{JY}}^{\mathrm{ZLYT}},\gamma_{\mathrm{JY}}^{\mathrm{ZLFB}},\gamma_{\mathrm{JY}}^{\mathrm{MP}},\gamma_{\mathrm{JY}}^{\mathrm{FLYT}},\gamma_{\mathrm{JY}}^{\mathrm{FLFB}},\gamma_{\mathrm{JY}}^{\mathrm{YL}},\gamma_{\mathrm{JY}}^{\mathrm{CH}},n_0,\delta,m\right) \\ g_2(\boldsymbol{X}) = E_B\left(E_1,\rho_1,\nu_1,E_2,\rho_2,\nu_2,\gamma_{\mathrm{JY}}^{\mathrm{ZLYT}},\gamma_{\mathrm{JY}}^{\mathrm{ZLFB}},\gamma_{\mathrm{JY}}^{\mathrm{MP}},\gamma_{\mathrm{JY}}^{\mathrm{FLYT}},\gamma_{\mathrm{JY}}^{\mathrm{FLFB}},\gamma_{\mathrm{JY}}^{\mathrm{YL}},\gamma_{\mathrm{JY}}^{\mathrm{CH}},n_0,\delta,m\right) \end{cases} \tag{48}$$

where E_1, ρ_1, and ν_1 represent the elastic modulus, density, and Poisson's ratio of the 30CrMnSiNi2A alloy steel, respectively. E_2, ρ_2, and ν_2 represent the elastic modulus, density, and Poisson's ratio of the 2024 aluminum alloy, respectively. $\gamma_{\mathrm{JY}}^{\mathrm{ZLYT}}$ and $\gamma_{\mathrm{JY}}^{\mathrm{ZLFB}}$ mean the main I-beam flange thickness and web thickness, respectively. $\gamma_{\mathrm{JY}}^{\mathrm{FLYT}}$ and $\gamma_{\mathrm{JY}}^{\mathrm{FLFB}}$ represent the auxiliary I-beam flange thickness and web thickness, respectively. $\gamma_{\mathrm{JY}}^{\mathrm{MP}}$, $\gamma_{\mathrm{JY}}^{\mathrm{YL}}$ and $\gamma_{\mathrm{JY}}^{\mathrm{CH}}$ are the thicknesses of the skin, wing rib, and long truss, respectively. n_0, δ and m represent the mobile overload, load correction factor and weight of the airplane, respectively. All these parameters are considered as random variables, and their corresponding distribution parameters are listed in table 20.

For the UP analysis of the airplane wing, tables 21 and 22 present the mean and standard deviation results obtained through various methods. Statistical moments, based on established analytical and univariate integral techniques, are illustrated in figure 22, and the PDFs for the two outputs are presented in figure 23. The actual mean and standard deviation results for stress at position A of the skeletal structure are 571.7182 MPa and 83.6428 MPa, respectively. For the strain solution at position B of the skin structure, the actual mean and standard deviation results are 0.0028 and 0.0004, respectively. Analyzing the statistical moments for stress at position A from table 21, it is evident that the proposed method provides relatively accurate estimations of the mean and standard deviation with a small computational cost. While the SGNI method offers the most accurate estimation of the mean, its relative error in estimating the standard deviation is large, and the computational cost is nearly tenfold that of the proposed method. Additionally, the Sobol method provides relatively accurate estimations of the mean and standard deviation, but the corresponding PDF exhibits a significant error, as shown in figure 23. Meanwhile, the FFNI method offers relatively

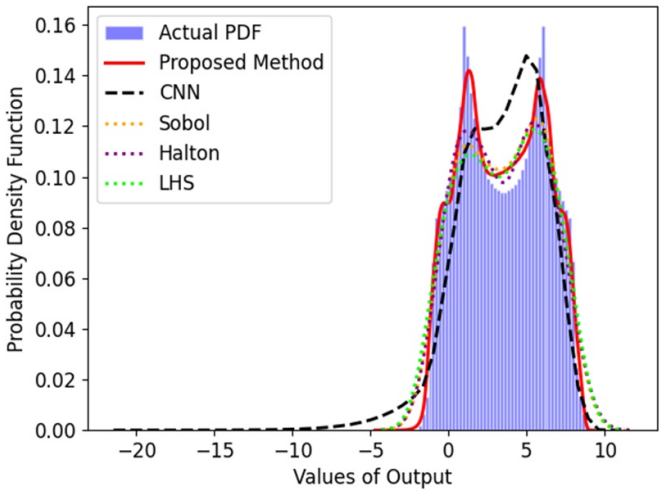

Figure 15. PDF of structural output for Case 3.

Table 4. Distribution parameters of random variables for the multiple outputs example.

Random variables	Distribution	Mean	Standard deviation
X_1	Normal	0.500	0.030
X_2	Normal	1.310	0.030
X_3	Normal	0.500	0.030
X_4	Normal	1.395	0.030
X_5	Normal	0.875	0.030
X_6	Normal	1.200	0.030
X_7	Normal	0.400	0.030
X_8	Normal	0.345	0.006
X_9	Normal	0.192	0.006
X_{10}	Normal	0	10
X_{11}	Normal	0	10

Table 5. Mean and standard deviation results for output 1.

Methods	Mean	$\Delta_\mu/\%$	Standard deviation	$\Delta_\sigma/\%$	N_{call}
FFNI	−0.5657	0.01	0.0447	0.71	31
SGNI ($q=3$)	−0.5657	0.00	0.0450	0.02	265
Sobol	−0.5685	0.49	0.0462	2.70	37
Halton	−0.5700	0.75	0.0461	2.38	
LHS	−0.5637	0.36	0.0533	18.38	
CNN	−0.5685	0.48	0.0408	9.41	
Proposed	−0.5653	0.08	0.0440	2.19	
MCS	−0.5657	—	0.0450	—	10^8

accurate estimations of the mean and standard deviation, but its limitation lies in the inability to provide a solution for the PDF, restricting its practical applicability.

For the statistical moments related to the strain solution at position B of the skin structure, table 21 indicates that all methods provide relatively accurate estimations, as evidenced by small absolute errors compared to the actual results.

Table 6. Mean and standard deviation results for output 2.

Methods	Mean	$\Delta_\mu/\%$	Standard deviation	$\Delta_\sigma/\%$	N_{call}
FFNI	−0.0929	0.01	0.0595	10.67	31
SGNI ($q=3$)	−0.0929	0.05	0.0666	0.02	265
Sobol	−0.0932	0.42	0.0651	2.26	273
Halton	−0.0901	2.98	0.0675	1.39	
LHS	−0.0928	0.02	0.0670	0.58	
CNN	−0.0936	0.85	0.0658	1.19	
Proposed	−0.0930	0.14	0.0663	0.41	
MCS	−0.0929	—	0.0666	—	10^8

Table 7. Mean and standard deviation results for output 3.

Methods	Mean	$\Delta_\mu/\%$	Standard deviation	$\Delta_\sigma/\%$	N_{call}
FFNI	−3.3972	0.01	0.8309	0.17	46
SGNI ($q=3$)	−3.3970	0.00	0.8295	0.01	265
Sobol	−3.3812	0.47	0.7993	3.64	78
Halton	−3.4558	1.73	0.8400	1.26	
LHS	−3.3935	0.10	0.8715	5.07	
CNN	−3.3859	0.33	0.8096	2.40	
Proposed	−3.4027	0.17	0.8304	0.11	
MCS	−3.3970	—	0.8294	—	10^8

Table 8. Mean and standard deviation results for output 4.

Methods	Mean	$\Delta_\mu/\%$	Standard deviation	$\Delta_\sigma/\%$	N_{call}
FFNI	−4.8689	0.01	1.6390	0.20	41
SGNI ($q=3$)	−4.8687	0.00	1.6358	0.00	265
Sobol	−4.8713	0.05	1.5827	3.24	103
Halton	−5.0132	2.97	1.6764	2.48	
LHS	−4.8625	0.13	1.6606	1.52	
CNN	−4.8746	0.12	1.6229	0.78	
Proposed	−4.8753	0.13	1.6314	0.27	
MCS	−4.8687	—	1.6358	—	10^8

Table 9. Mean and standard deviation results for output 5.

Methods	Mean	$\Delta_\mu/\%$	Standard deviation	$\Delta_\sigma/\%$	N_{call}
FFNI	−0.8343	0.00	0.6818	5.83	26
SGNI ($q=3$)	−0.8343	0.01	0.6442	0.00	265
Sobol	−0.8333	0.11	0.6482	0.63	272
Halton	−0.8563	2.65	0.6502	0.94	
LHS	−0.8344	0.01	0.6618	2.73	
CNN	−0.8340	0.04	0.6391	0.79	
Proposed	−0.8371	0.34	0.6445	0.05	
MCS	−0.8343	—	0.6442	—	10^8

Figure 22 reveals a close alignment between simulated results and the calculated mean (from established analytical technique) and standard deviation (from the established univariate integral technique) when a sufficient number of samples are used. This observation emphasizes the efficacy of

066

Table 10. Mean and standard deviation results for output 6.

Methods	Mean	$\Delta_\mu/\%$	Standard deviation	$\Delta_\sigma/\%$	N_{call}
FFNI	−0.1055	0.00	0.0081	0.55	36
SGNI (q = 3)	−0.1055	0.00	0.0082	0.81	265
Sobol	−0.1055	0.02	0.0082	0.06	32
Halton	−0.1057	0.17	0.0084	3.35	
LHS	−0.1054	0.11	0.0087	6.82	
CNN	−0.1055	0.03	0.0079	2.95	
Proposed	−0.1056	0.12	0.0079	3.18	
MCS	−0.1055	—	0.0081	—	10^8

Table 11. Mean and standard deviation results for output 7.

Methods	Mean	$\Delta_\mu/\%$	Standard deviation	$\Delta_\sigma/\%$	N_{call}
FFNI	−0.0775	0.00	0.0049	0.00	51
SGNI ($q = 3$)	−0.0775	0.05	0.0049	0.54	265
Sobol	−0.0773	0.27	0.0054	9.56	37
Halton	−0.0784	1.06	0.0052	5.28	
LHS	−0.0775	0.02	0.0053	7.96	
CNN	−0.0769	0.87	0.0041	15.87	
Proposed	−0.0778	0.39	0.0045	8.49	
MCS	−0.0775	—	0.0049	—	10^8

Table 12. Mean and standard deviation results for output 8.

Methods	Mean	$\Delta_\mu/\%$	Standard deviation	$\Delta_\sigma/\%$	N_{call}
FFNI	−0.0302	0.02	0.0065	0.01	31
SGNI (q = 3)	−0.0302	0.02	0.0065	0.34	265
Sobol	−0.0300	0.56	0.0062	4.63	89
Halton	−0.0304	0.61	0.0070	6.42	
LHS	−0.0303	0.34	0.0068	3.67	
CNN	−0.0302	0.19	0.0064	2.55	
Proposed	−0.0301	0.27	0.0065	0.54	
MCS	−0.0302	—	0.0065	—	10^8

Table 13. Mean and standard deviation results for output 9.

Methods	Mean	$\Delta_\mu/\%$	Standard deviation	$\Delta_\sigma/\%$	N_{call}
FFNI	−0.6428	0.01	0.1696	0.07	36
SGNI (q = 3)	−0.6428	0.00	0.1697	0.01	265
Sobol	−0.6430	0.04	0.1612	5.00	108
Halton	−0.6543	1.80	0.1679	1.07	
LHS	−0.6414	0.21	0.1614	4.91	
CNN	−0.6431	0.04	0.1715	1.04	
Proposed	−0.6442	0.23	0.1693	0.26	
MCS	−0.6428	—	0.1697	—	10^8

both established analytical and univariate integral techniques. Furthermore, the PDFs in figure 23 emphasize that the proposed method excels in providing the most accurate estimations of the PDF for output 1 and relatively accurate estimations for output 2. This illustrates the effectiveness of the proposed method in addressing the UP of the airplane wing.

Table 14. Mean and standard deviation results for output 10.

Methods	Mean	$\Delta_\mu/\%$	Standard deviation	$\Delta_\sigma/\%$	N_{call}
FFNI	−0.3016	0.02	0.2088	16.44	36
SGNI (q = 3)	−0.3016	0.02	0.1793	0.00	265
Sobol	−0.3021	0.20	0.1775	1.01	261
Halton	−0.3003	0.42	0.1741	2.92	
LHS	−0.3010	0.17	0.1752	2.26	
CNN	−0.2989	0.89	0.1759	1.88	
Proposed	−0.3005	0.35	0.1771	1.22	
MCS	−0.3015	—	0.1793	—	10^8

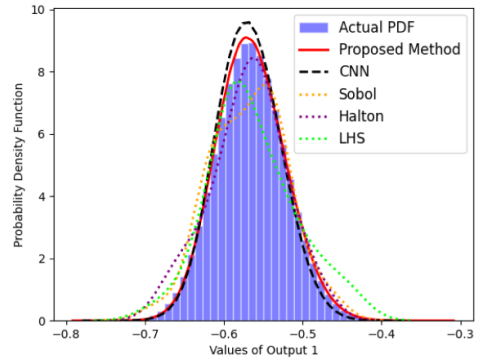

(a) PDF of output 1

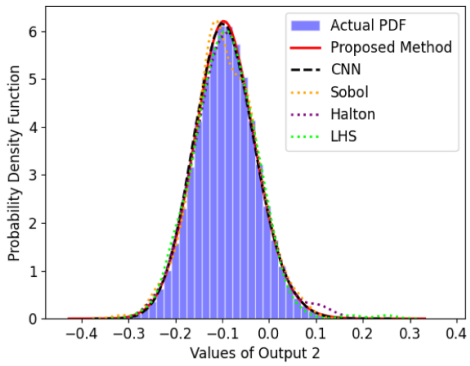

(b) PDF of output 2

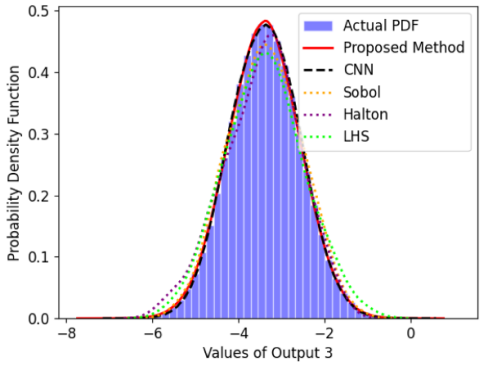

(c) PDF of output 3

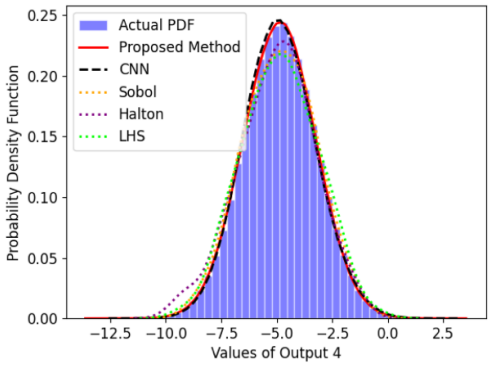

(d) PDF of output 4

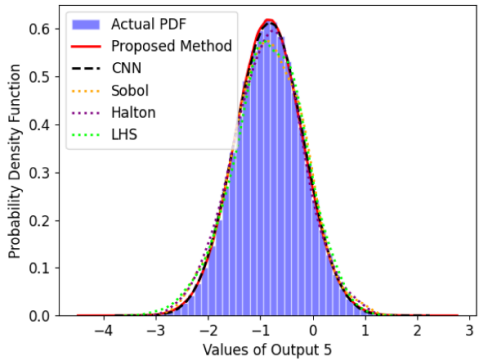

(e) PDF of output 5

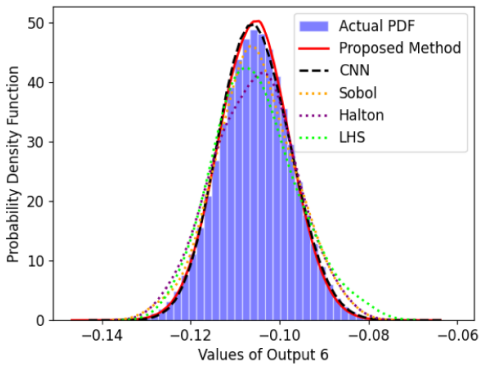

(f) PDF of output 6

Figure 16. PDFs of structural outputs for the multiple outputs example.

068

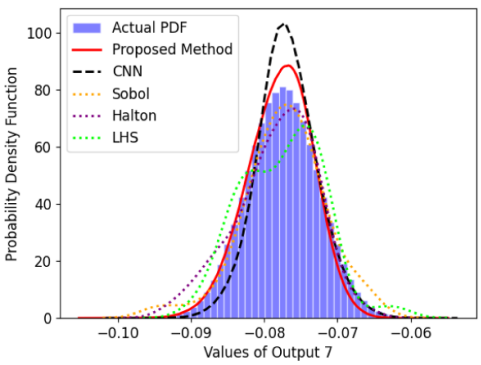

(g) PDF of output 7

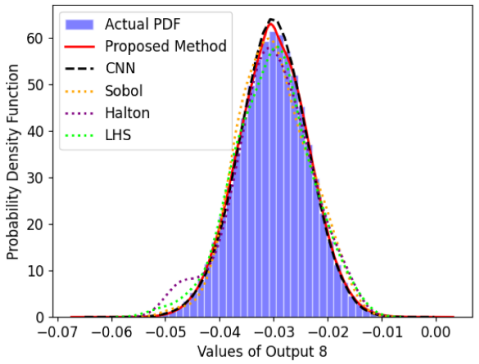

(h) PDF of output 8

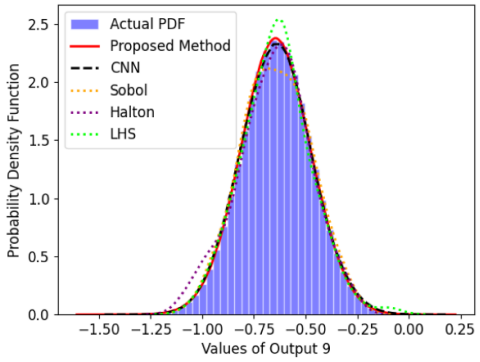

(i) PDF of output 9

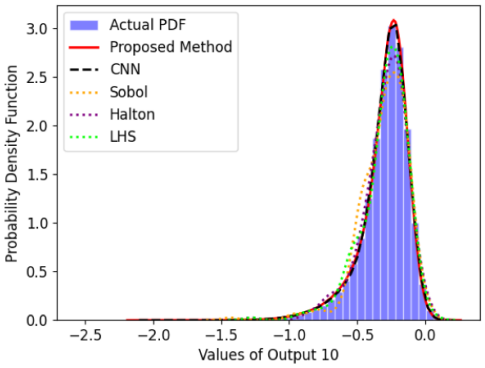

(j) PDF of output 10

Figure 16. (Continued.)

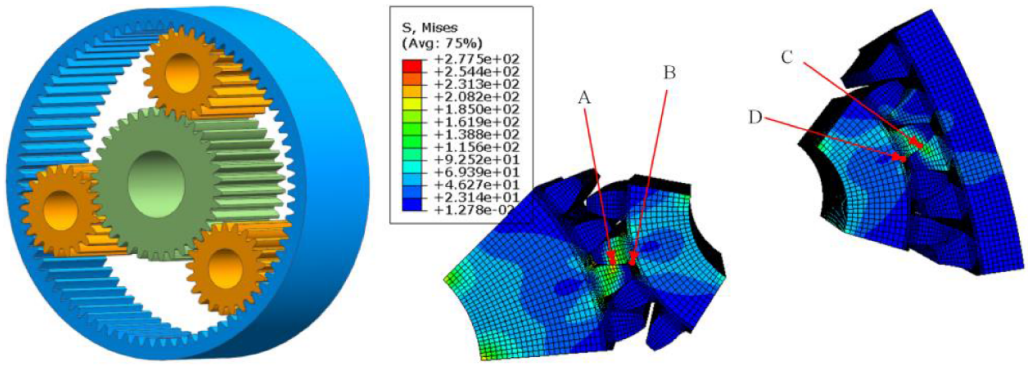

(a) The geometric model (b) The stress analysis solution

Figure 17. The planetary transmission gear.

Table 15. Distribution parameters of random variables for the planetary transmission gear.

Random variables	Distribution	Para1	Para2
E/ (Mpa)	Lognormal	210 000	10 500
ν	Truncated Normal	0.3	0.015
m	Truncated Normal	0.05	0.0025
T/ (Nmm)	Uniform	290 000	310 000

Note: For the lognormal and truncated normal distributions, para1 and para2 represent the mean and standard deviation, respectively. For the uniform distribution, para1 and para2 mean the lower and upper bounds, respectively. The value range of the truncated normal distribution is between positive and negative 3 sigma intervals.

Table 16. Mean and standard deviation results for output 1 of the planetary transmission gear.

Methods	Mean	$\Delta_\mu/\%$	Standard deviation	$\Delta_\sigma/\%$	N_{call}
FFNI	175.0194	0.01	3.9110	1.75	21
SGNI (q = 3)	175.0171	0.01	3.9000	2.03	41
Sobol	174.8409	0.12	3.7005	7.04	16
Halton	175.1575	0.07	4.0002	0.49	
LHS	174.8409	0.04	4.4768	12.46	
CNN	175.1300	0.05	4.4429	11.61	
Proposed	174.8739	0.10	3.9203	1.52	
MCS	175.0424	—	3.9808	—	10^4

Table 17. Mean and standard deviation results for output 2 of the planetary transmission gear.

Methods	Mean	$\Delta_\mu/\%$	Standard deviation	$\Delta_\sigma/\%$	N_{call}
FFNI	224.8637	0.01	5.6579	1.35	21
SGNI ($q = 3$)	224.8607	0.01	5.6666	1.20	41
Sobol	224.6384	0.11	5.6099	2.19	16
Halton	224.9185	0.01	5.6755	1.04	
LHS	224.6384	0.03	6.3426	10.59	
CNN	224.9079	0.01	5.4069	5.73	
Proposed	224.7336	0.07	5.7565	0.37	
MCS	224.8889	—	5.7353	—	10^4

Table 18. Mean and standard deviation results for output 3 of the planetary transmission gear.

Methods	Mean	$\Delta_\mu/\%$	Standard deviation	$\Delta_\sigma/\%$	N_{call}
FFNI	126.1454	0.01	2.8309	2.08	21
SGNI (q = 3)	126.1439	0.02	2.8180	2.53	41
Sobol	125.9911	0.14	2.6466	8.46	16
Halton	126.3097	0.12	2.8754	0.54	
LHS	125.9911	0.04	3.3137	14.62	
CNN	126.0247	0.11	2.7772	3.94	
Proposed	126.0410	0.10	2.8224	2.38	
MCS	126.1630	—	2.8911	—	10^4

Table 19. Mean and standard deviation results for output 4 of the planetary transmission gear.

Methods	Mean	$\Delta_\mu/\%$	Standard deviation	$\Delta_\sigma/\%$	N_{call}
FFNI	211.3341	0.02	4.9354	1.34	21
SGNI ($q = 3$)	211.3314	0.02	4.9323	1.41	41
Sobol	211.1413	0.11	4.7312	5.43	16
Halton	211.3514	0.01	5.0702	1.35	
LHS	211.1413	0.03	5.4384	8.71	
CNN	211.0877	0.14	4.8958	2.14	
Proposed	211.1638	0.10	4.9503	1.05	
MCS	211.3735	—	5.0028	—	10^4

070

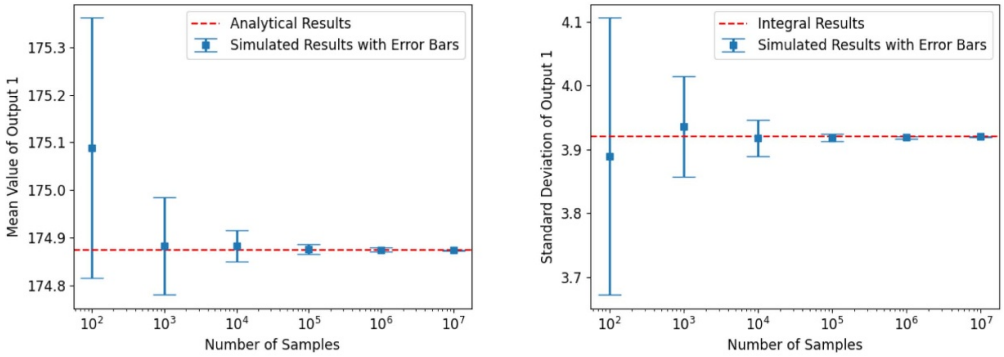

(a) Mean of output 1

(b) Standard deviation of output 1

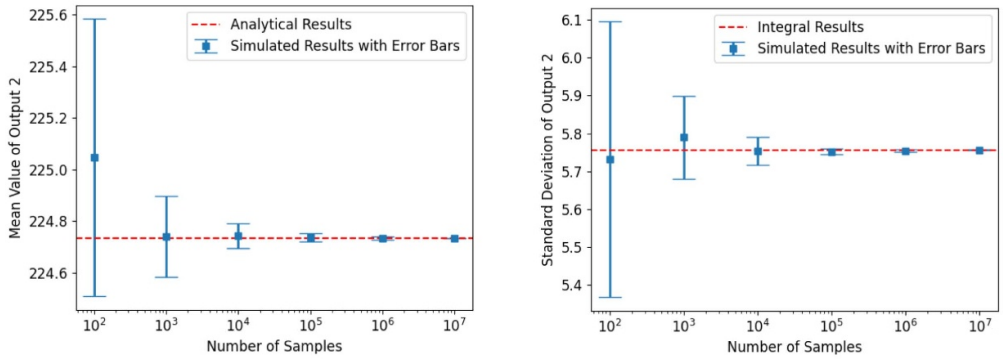

(c) Mean of output 2

(d) Standard deviation of output 2

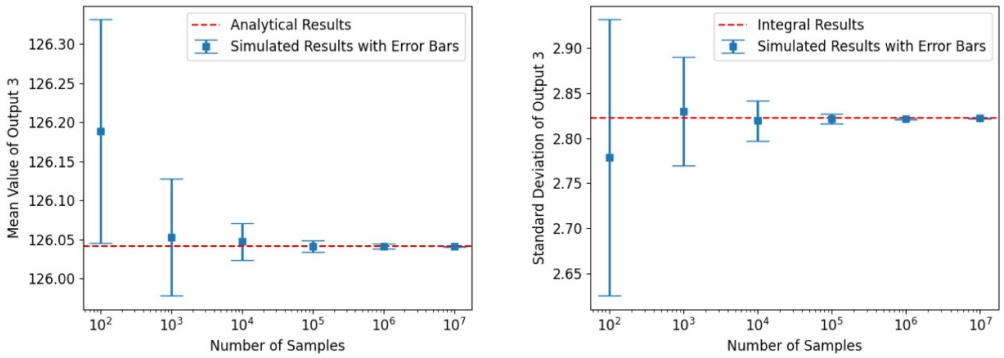

(e) Mean of output 3

(f) Standard deviation of output 3

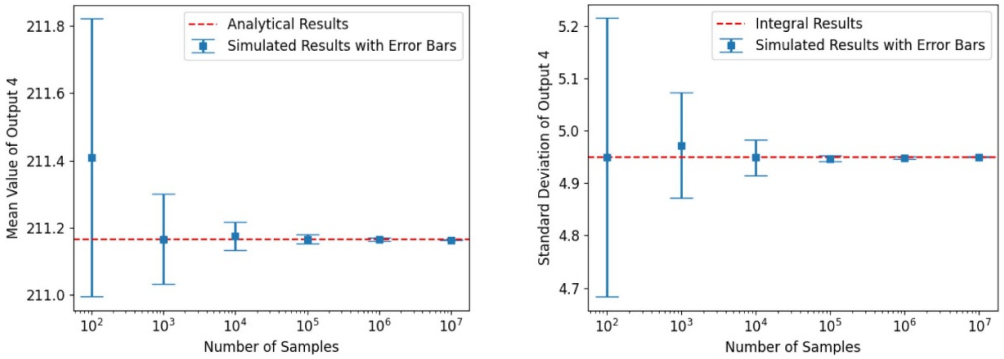

(g) Mean of output 4

(h) Standard deviation of output 4

Figure 18. Predicted statistical moments for outputs of the planetary transmission gear.

071

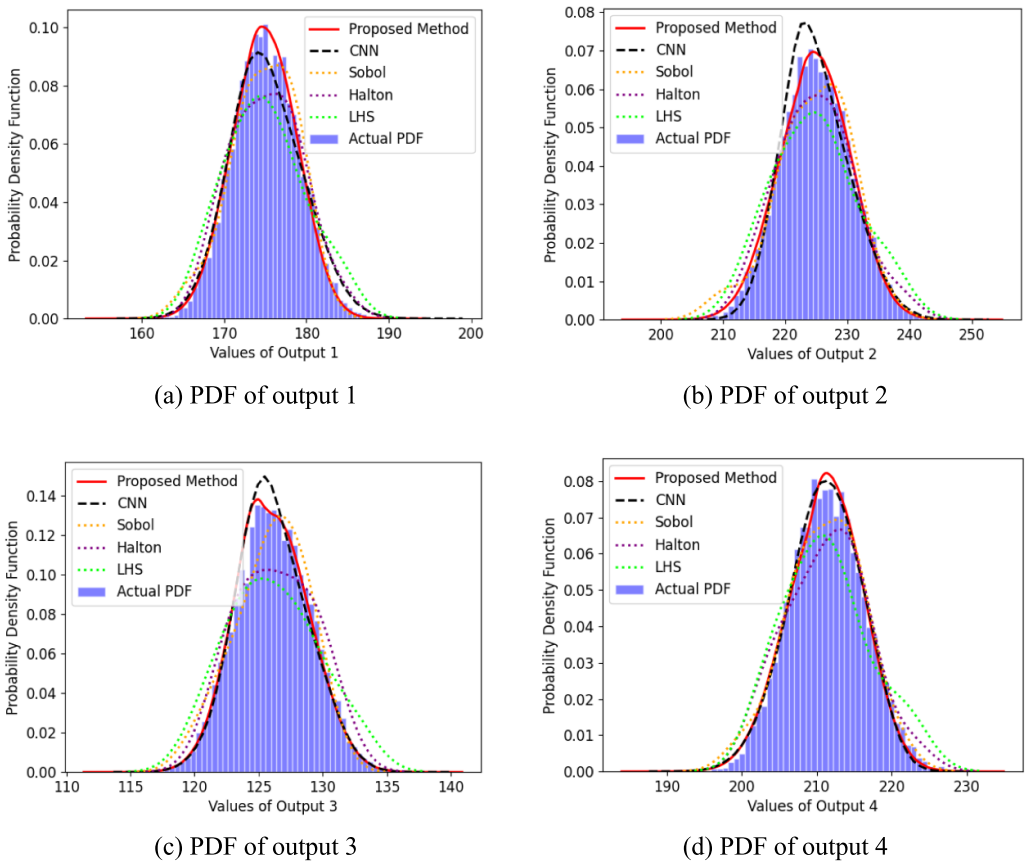

(a) PDF of output 1 (b) PDF of output 2

(c) PDF of output 3 (d) PDF of output 4

Figure 19. PDFs of structural outputs for the planetary transmission gear.

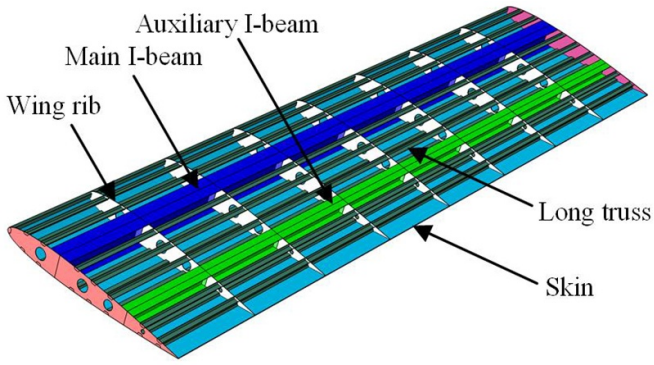

Figure 20. The airplane wing.

5. Conclusions

In conclusion, this work introduces a novel adaptive method based on the ANN to address structural UP issues. The method utilizes analytical derivation of output means through the ANN, facilitating direct computation via network weight and bias vectors. The standard deviation of outputs is determined using an established efficient technique, employing univariate integrals instead of multivariate integrals. The analytical and univariate integral techniques effectively alleviate post-processing errors commonly associated with numerical simulation techniques for estimating statistical moments within the ANN framework. Furthermore, an adaptive framework that incorporates input space division and an adjustable multi-point addition strategy is proposed in this work. This framework enhances the computational accuracy of the analytical and univariate integral techniques for estimating statistical moments of outputs.

072

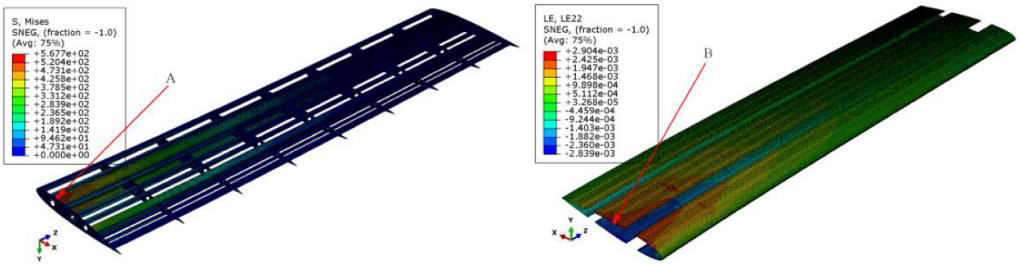

(a) Skeleton structure (b) Skin structure

Figure 21. Performance of the airplane wing.

Table 20. Distribution parameters of random variables for the airplane wing.

Random variables	Distribution	Para1	Para2
E_1 (Mpa)	Lognormal	207 000	10 350
ρ_1 $\left(\text{ton mm}^{-3}\right)$	Truncated Normal	7.77×10^{-9}	3.885×10^{-10}
ν_1	Truncated Normal	0.3	0.015
E_2 (Mpa)	Lognormal	68 000	3400
ρ_2 $\left(\text{ton mm}^{-3}\right)$	Truncated Normal	2.8×10^{-9}	1.4×10^{-10}
ν_2	Truncated Normal	0.3	0.015
$\gamma_{\text{JY}}^{\text{ZLYT}}$ (mm)	Truncated Normal	30	1.5
$\gamma_{\text{JY}}^{\text{ZLFB}}$ (mm)	Truncated Normal	25	1.25
$\gamma_{\text{JY}}^{\text{FLYT}}$ (mm)	Truncated Normal	20	1
$\gamma_{\text{JY}}^{\text{FLFB}}$ (mm)	Truncated Normal	15	0.75
$\gamma_{\text{JY}}^{\text{YL}}$ (mm)	Truncated Normal	10	0.5
$\gamma_{\text{JY}}^{\text{CH}}$ (mm)	Truncated Normal	4	0.2
$\gamma_{\text{JY}}^{\text{MP}}$ (mm)	Truncated Normal	3.5	0.175
n_0 $\left(\text{mm s}^{-2}\right)$	Uniform	9800	14 700
δ	Uniform	1.003 58	1.023 88
m (ton)	Truncated Normal	20	1

Table 21. Mean and standard deviation results for output 1 of the airplane wing.

Methods	Mean	$\Delta_\mu/\%$	Standard deviation	$\Delta_\sigma/\%$	N_{call}
FFNI	572.9809	0.22	82.4081	1.48	81
SGNI ($q = 3$)	571.8159	0.02	79.4675	4.99	545
Sobol	572.7671	0.18	83.5025	0.17	56
Halton	572.9475	0.22	88.5600	5.88	
LHS	573.7503	0.36	87.5737	4.70	
CNN	573.0486	0.48	79.4465	6.41	
Proposed	572.9064	0.21	80.8171	3.37	
MCS	571.7182	—	83.6428	—	10^4

Table 22. Mean and standard deviation results for output 2 of the airplane wing.

Methods	Mean	$\Delta_\mu/\%$	Standard deviation	$\Delta_\sigma/\%$	N_{call}
FFNI	0.0029	1.81	0.0004	5.51	81
SGNI ($q = 3$)	0.0028	1.60	0.0004	2.31	545
Sobol	0.0029	0.25	0.0005	9.63	57
Halton	0.0029	0.57	0.0004	4.62	
LHS	0.0029	0.55	0.0005	9.94	
CNN	0.0028	0.22	0.0004	9.72	
Proposed	0.0029	0.27	0.0004	4.82	
MCS	0.0028	—	0.0004	—	10^4

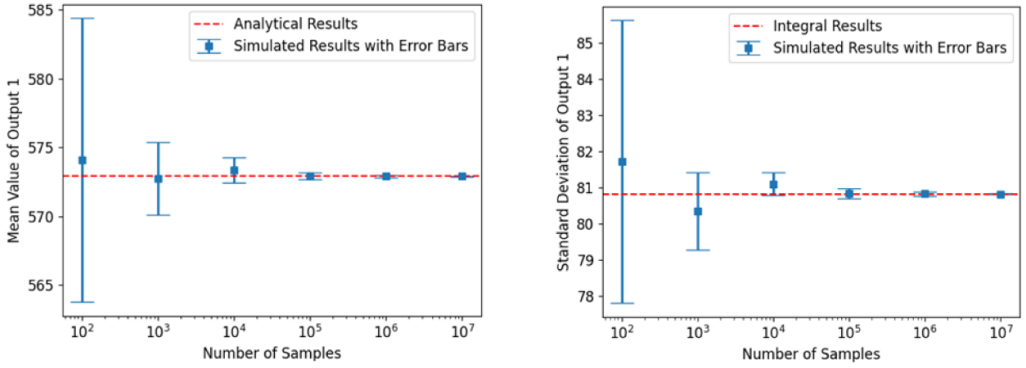

(a) Mean of output 1 (b) Standard deviation of output 1

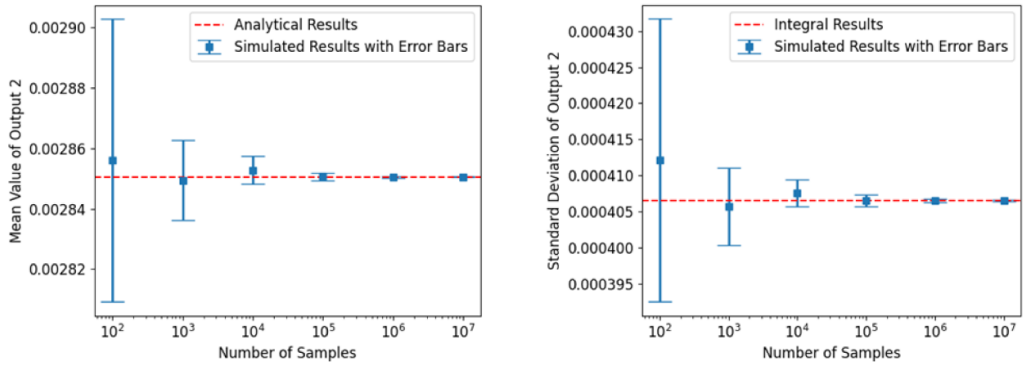

(c) Mean of output 2 (d) Standard deviation of output 2

Figure 22. Predicted statistical moments for outputs of the airplane wing.

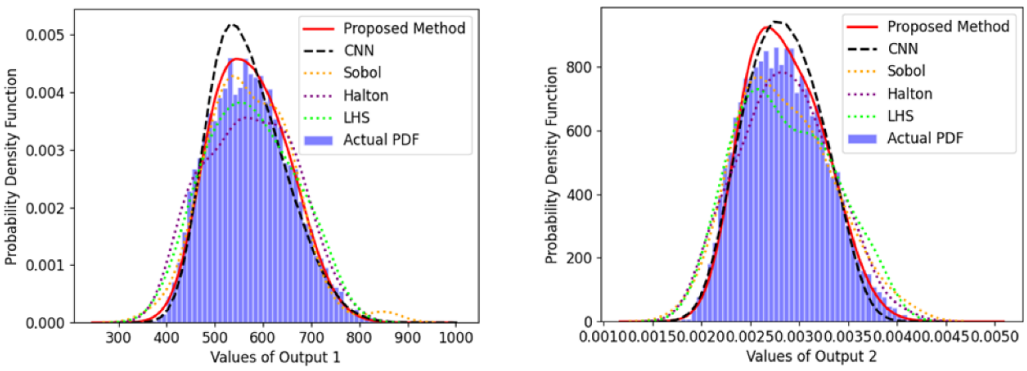

(a) PDF of output 1 (b) PDF of output 2

Figure 23. PDFs of structural outputs for the airplane wing.

The proposed method is demonstrated across various applications, including highly nonlinear scenarios, multiple outputs, and cases involving finite element models. To validate its efficacy, we compare the proposed method with several widely used methods, including LHS, Sobol sequences, Halton series, FFNI, SGNI, CNN, and MCS. The results consistently show that the proposed method not only provides accurate estimations of statistical moments but also offers effective estimations of the PDF for structural outputs. In summary, the introduced adaptive method demonstrates robust performance across diverse scenarios, showcasing its potential as a reliable and efficient tool for addressing structural UP challenges.

However, the proposed approach utilizes an ANN structure with a single hidden layer and ReLU activation function. Future work will focus on extending this method to ANN architectures with multiple hidden layers and exploring alternative activation functions, such as the Tanh function [67].

074

Acknowledgment

This work is supported by the National Natural Science Foundation of China (Grants 52205252 and 72331002), and the National Natural Science Foundation of Sichuan Province (Grant 2023NSFSC0876). The first author would also thanks for the support of the Alexander von Humboldt Foundation of Germany.

Conflict of interest

The authors declare that they have no conflict of interest.

Appendix A

Let $t = \frac{Y_{\mathrm{ReLU}l} - \mu_{Y_{\mathrm{HI}}}}{\sigma_{Y_{\mathrm{HI}}}}$, then the mean of the response $Y_{\mathrm{ReLU}l}$ can be rewritten as follows:

$$\mu_{Y_{\mathrm{ReLU}l}} = \frac{1}{\sqrt{2\pi}} \int_{-\frac{\mu_{Y_{\mathrm{HI}}}}{\sigma_{Y_{\mathrm{HI}}}}}^{+\infty} (\sigma_{Y_{\mathrm{HI}}} t + \mu_{Y_{\mathrm{HI}}}) \exp\left\{-\frac{t^2}{2}\right\} \mathrm{d}t = \frac{\sigma_{Y_{\mathrm{HI}}}}{\sqrt{2\pi}} \int_{-\frac{\mu_{Y_{\mathrm{HI}}}}{\sigma_{Y_{\mathrm{HI}}}}}^{+\infty} t \exp\left\{-\frac{t^2}{2}\right\} \mathrm{d}t + \frac{\mu_{Y_{\mathrm{HI}}}}{\sqrt{2\pi}} \int_{-\frac{\mu_{Y_{\mathrm{HI}}}}{\sigma_{Y_{\mathrm{HI}}}}}^{+\infty} \exp\left\{-\frac{t^2}{2}\right\} \mathrm{d}t \tag{A-1}$$

in which

$$\frac{\sigma_{Y_{\mathrm{HI}}}}{\sqrt{2\pi}} \int_{-\frac{\mu_{Y_{\mathrm{HI}}}}{\sigma_{Y_{\mathrm{HI}}}}}^{+\infty} t \exp\left\{-\frac{t^2}{2}\right\} \mathrm{d}t = -\frac{\sigma_{Y_{\mathrm{HI}}}}{\sqrt{2\pi}} \exp\left\{-\frac{t^2}{2}\right\} \Big|_{-\frac{\mu_{Y_{\mathrm{HI}}}}{\sigma_{Y_{\mathrm{HI}}}}}^{+\infty} = \sigma_{Y_{\mathrm{HI}}} \phi\left(-\frac{\mu_{Y_{\mathrm{HI}}}}{\sigma_{Y_{\mathrm{HI}}}}\right) \tag{A-2}$$

$$\frac{\mu_{Y_{\mathrm{HI}}}}{\sqrt{2\pi}} \int_{-\frac{\mu_{Y_{\mathrm{HI}}}}{\sigma_{Y_{\mathrm{HI}}}}}^{+\infty} \exp\left\{-\frac{t^2}{2}\right\} \mathrm{d}t = \mu_{Y_{\mathrm{HI}}} \left[1 - \Phi\left(-\frac{\mu_{Y_{\mathrm{HI}}}}{\sigma_{Y_{\mathrm{HI}}}}\right)\right] \tag{A-3}$$

where $\Phi(\cdot)$ and $\phi(\cdot)$ represent the CDF and PDF of standard normal variables, respectively. Therefore, the analytical solution of the mean of the response $Y_{\mathrm{ReLU}l}$ can be obtained by:

$$\mu_{Y_{\mathrm{ReLU}l}} = \mu_{Y_{\mathrm{HI}}} \left[1 - \Phi\left(-\frac{\mu_{Y_{\mathrm{HI}}}}{\sigma_{Y_{\mathrm{HI}}}}\right)\right] + \sigma_{Y_{\mathrm{HI}}} \phi\left(-\frac{\mu_{Y_{\mathrm{HI}}}}{\sigma_{Y_{\mathrm{HI}}}}\right). \tag{A-4}$$

Appendix B

Let $t = \frac{Y_{\mathrm{ReLU}l} - \mu_{Y_{\mathrm{HI}}}}{\sigma_{Y_{\mathrm{HI}}}}$, then the standard deviation of the response $Y_{\mathrm{ReLU}l}$ can be rewritten as follows:

$$\begin{aligned}
\sigma_{Y_{\mathrm{ReLU}l}} &= \sqrt{\frac{1}{\sqrt{2\pi}} \int_{-\frac{\mu_{Y_{\mathrm{HI}}}}{\sigma_{Y_{\mathrm{HI}}}}}^{+\infty} (\sigma_{Y_{\mathrm{HI}}} t + \mu_{Y_{\mathrm{HI}}})^2 \exp\left\{-\frac{t^2}{2}\right\} \mathrm{d}t - \mu_{Y_{\mathrm{ReLU}l}}^2} \\
&= \sqrt{\frac{\sigma_{Y_{\mathrm{HI}}}^2}{\sqrt{2\pi}} \int_{-\frac{\mu_{Y_{\mathrm{HI}}}}{\sigma_{Y_{\mathrm{HI}}}}}^{+\infty} t^2 \exp\left\{-\frac{t^2}{2}\right\} \mathrm{d}t + \frac{2\mu_{Y_{\mathrm{HI}}}\sigma_{Y_{\mathrm{HI}}}}{\sqrt{2\pi}} \int_{-\frac{\mu_{Y_{\mathrm{HI}}}}{\sigma_{Y_{\mathrm{HI}}}}}^{+\infty} t \exp\left\{-\frac{t^2}{2}\right\} \mathrm{d}t + \frac{\mu_{Y_{\mathrm{HI}}}^2}{\sqrt{2\pi}} \int_{-\frac{\mu_{Y_{\mathrm{HI}}}}{\sigma_{Y_{\mathrm{HI}}}}}^{+\infty} \exp\left\{-\frac{t^2}{2}\right\} \mathrm{d}t - \mu_{Y_{\mathrm{ReLU}l}}^2}
\end{aligned} \tag{B-1}$$

where

$$\frac{\sigma_{Y_{\mathrm{HI}}}^2}{\sqrt{2\pi}}\int_{-\frac{\mu_{Y_{\mathrm{HI}}}}{\sigma_{Y_{\mathrm{HI}}}}}^{+\infty} t^2\exp\left\{-\frac{t^2}{2}\right\}\mathrm{d}t=-\frac{\sigma_{Y_{\mathrm{HI}}}^2}{\sqrt{2\pi}}\int_{-\frac{\mu_{Y_{\mathrm{HI}}}}{\sigma_{Y_{\mathrm{HI}}}}}^{+\infty} t\mathrm{d}\exp\left\{-\frac{t^2}{2}\right\}=-\frac{\sigma_{Y_{\mathrm{HI}}}^2}{\sqrt{2\pi}}\left\{t\exp\left\{-\frac{t^2}{2}\right\}\Big|_{-\frac{\mu_{Y_{\mathrm{HI}}}}{\sigma_{Y_{\mathrm{HI}}}}}^{+\infty}-\int_{-\frac{\mu_{Y_{\mathrm{HI}}}}{\sigma_{Y_{\mathrm{HI}}}}}^{+\infty}\exp\left\{-\frac{t^2}{2}\right\}\mathrm{d}t\right\}$$
$$=-\frac{\mu_{Y_{\mathrm{HI}}}}{\sigma_{Y_{\mathrm{HI}}}}\sigma_{Y_{\mathrm{HI}}}^2\phi\left(-\frac{\mu_{Y_{\mathrm{HI}}}}{\sigma_{Y_{\mathrm{HI}}}}\right)+\sigma_{Y_{\mathrm{HI}}}^2\left[1-\Phi\left(-\frac{\mu_{Y_{\mathrm{HI}}}}{\sigma_{Y_{\mathrm{HI}}}}\right)\right] \tag{B-2}$$

$$\frac{2\mu_{Y_{\mathrm{HI}}}\sigma_{Y_{\mathrm{HI}}}}{\sqrt{2\pi}}\int_{-\frac{\mu_{Y_{\mathrm{HI}}}}{\sigma_{Y_{\mathrm{HI}}}}}^{+\infty} t\exp\left\{-\frac{t^2}{2}\right\}\mathrm{d}t=2\mu_{Y_{\mathrm{HI}}}\sigma_{Y_{\mathrm{HI}}}\phi\left(-\frac{\mu_{Y_{\mathrm{HI}}}}{\sigma_{Y_{\mathrm{HI}}}}\right) \tag{B-3}$$

$$\frac{\mu_{Y_{\mathrm{HI}}}^2}{\sqrt{2\pi}}\int_{-\frac{\mu_{Y_{\mathrm{HI}}}}{\sigma_{Y_{\mathrm{HI}}}}}^{+\infty}\exp\left\{-\frac{t^2}{2}\right\}\mathrm{d}t=\mu_{Y_{\mathrm{HI}}}^2\left[1-\Phi\left(-\frac{\mu_{Y_{\mathrm{HI}}}}{\sigma_{Y_{\mathrm{HI}}}}\right)\right]. \tag{B-4}$$

Substituting equations (B-2)–(B-4) into equation (B-1), the standard deviation of the response $Y_{\mathrm{ReLU}l}$ can be further expressed by:

$$\sigma_{Y_{\mathrm{ReLU}l}}=\sqrt{-\frac{\mu_{Y_{\mathrm{HI}}}}{\sigma_{Y_{\mathrm{HI}}}}\sigma_{Y_{\mathrm{HI}}}^2\phi\left(-\frac{\mu_{Y_{\mathrm{HI}}}}{\sigma_{Y_{\mathrm{HI}}}}\right)+\sigma_{Y_{\mathrm{HI}}}^2\left[1-\Phi\left(-\frac{\mu_{Y_{\mathrm{HI}}}}{\sigma_{Y_{\mathrm{HI}}}}\right)\right]+2\mu_{Y_{\mathrm{HI}}}\sigma_{Y_{\mathrm{HI}}}\phi\left(-\frac{\mu_{Y_{\mathrm{HI}}}}{\sigma_{Y_{\mathrm{HI}}}}\right)+\mu_{Y_{\mathrm{HI}}}^2\left[1-\Phi\left(-\frac{\mu_{Y_{\mathrm{HI}}}}{\sigma_{Y_{\mathrm{HI}}}}\right)\right]-\mu_{Y_{\mathrm{ReLU}l}}^2}. \tag{B-5}$$

Furthermore, by substituting equation (A-4) into equation (B-5), the analytical solution of standard deviation of the response $Y_{\mathrm{ReLU}l}$ can be obtained as follows:

$$\sigma_{Y_{\mathrm{ReLU}l}}=\sqrt{\frac{\mu_{Y_{\mathrm{HI}}}}{\sigma_{Y_{\mathrm{HI}}}}\sigma_{Y_{\mathrm{HI}}}^2\phi\left(-\frac{\mu_{Y_{\mathrm{HI}}}}{\sigma_{Y_{\mathrm{HI}}}}\right)+\sigma_{Y_{\mathrm{HI}}}^2+\left(\mu_{Y_{\mathrm{HI}}}^2-\sigma_{Y_{\mathrm{HI}}}^2\right)\Phi\left(-\frac{\mu_{Y_{\mathrm{HI}}}}{\sigma_{Y_{\mathrm{HI}}}}\right)-\left[\mu_{Y_{\mathrm{HI}}}\Phi\left(-\frac{\mu_{Y_{\mathrm{HI}}}}{\sigma_{Y_{\mathrm{HI}}}}\right)-\sigma_{Y_{\mathrm{HI}}}\phi\left(-\frac{\mu_{Y_{\mathrm{HI}}}}{\sigma_{Y_{\mathrm{HI}}}}\right)\right]^2}. \tag{B-6}$$

Appendix C

Let $u=\frac{Y_{\mathrm{ReLU}l_1}-\mu_{Y_{\mathrm{HI}_1}}}{\sqrt{2}\sigma_{Y_{\mathrm{HI}_1}}}-\rho_{l_1l_2}\frac{Y_{\mathrm{ReLU}l_2}-\mu_{Y_{\mathrm{HI}_2}}}{\sqrt{2}\sigma_{Y_{\mathrm{HI}_2}}}$ and $v=\sqrt{1-\rho_{l_1l_2}^2}\frac{Y_{\mathrm{ReLU}l_2}-\mu_{Y_{\mathrm{HI}_2}}}{\sqrt{2}\sigma_{Y_{\mathrm{HI}_2}}}$, then the variables $Y_{\mathrm{ReLU}l_1}$ and $Y_{\mathrm{ReLU}l_2}$ can be expressed by:

$$Y_{\mathrm{ReLU}l_1}=\sqrt{2}\sigma_{Y_{\mathrm{HI}_1}}u+\frac{\sqrt{2}\rho_{l_1l_2}\sigma_{Y_{\mathrm{HI}_1}}}{\sqrt{1-\rho_{l_1l_2}^2}}v+\mu_{Y_{\mathrm{HI}_1}} \tag{C-1}$$

$$Y_{\mathrm{ReLU}l_2}=\frac{\sqrt{2}\rho_{l_1l_2}\sigma_{Y_{\mathrm{HI}_2}}}{\sqrt{1-\rho_{l_1l_2}^2}}v+\mu_{Y_{\mathrm{HI}_2}}. \tag{C-2}$$

The Jacobin matrix is calculated as follows:

$$J=\begin{pmatrix}\frac{\partial Y_{\mathrm{ReLU}l_1}}{\partial u} & \frac{\partial Y_{\mathrm{ReLU}l_1}}{\partial v}\\ \frac{\partial Y_{\mathrm{ReLU}l_2}}{\partial u} & \frac{\partial Y_{\mathrm{ReLU}l_2}}{\partial v}\end{pmatrix}=\begin{pmatrix}\sqrt{2}\sigma_{Y_{\mathrm{HI}_1}} & \frac{\sqrt{2}\rho_{l_1l_2}\sigma_{Y_{\mathrm{HI}_1}}}{\sqrt{1-\rho_{l_1l_2}^2}}\\ 0 & \frac{\sqrt{2}\rho_{l_1l_2}\sigma_{Y_{\mathrm{HI}_2}}}{\sqrt{1-\rho_{l_1l_2}^2}}\end{pmatrix}. \tag{C-3}$$

The Jacobin determinant is shown below:

$$|J|=\frac{2\sigma_{Y_{\mathrm{HI}_1}}\sigma_{Y_{\mathrm{HI}_2}}}{\sqrt{1-\rho_{l_1l_2}^2}}. \tag{C-4}$$

076

Therefore, the two-dimensional integral shown in equation (28) can be transformed as follows:

$$\begin{aligned} E\left(Y_{\mathrm{ReLU}l_1}Y_{\mathrm{ReLU}l_2}\right) &= \int_{-\frac{\sqrt{1-\rho_{l_1l_2}^2}\mu_{Y_{\mathrm{HI}_2}}}{\sqrt{2}\sigma_{Y_{\mathrm{HI}_2}}}}^{+\infty}\int_{-\frac{\mu_{Y_{\mathrm{HI}_1}}}{\sqrt{2}\sigma_{Y_{\mathrm{HI}_1}}}-\frac{\rho_{l_1l_2}v}{\sqrt{1-\rho_{l_1l_2}^2}}}^{+\infty}\frac{1}{2\pi\sigma_{Y_{\mathrm{HI}_1}}\sigma_{Y_{\mathrm{HI}_2}}\sqrt{1-\rho_{l_1l_2}^2}}\exp\left\{-\frac{u^2+v^2}{1-\rho_{l_1l_2}^2}\right\} \\ &\times\left(\sqrt{2}\sigma_{Y_{\mathrm{HI}_1}}u+\frac{\sqrt{2}\rho_{l_1l_2}\sigma_{Y_{\mathrm{HI}_1}}}{\sqrt{1-\rho_{l_1l_2}^2}}v+\mu_{Y_{\mathrm{HI}_1}}\right)\left(\frac{\sqrt{2}\rho_{l_1l_2}\sigma_{Y_{\mathrm{HI}_2}}}{\sqrt{1-\rho_{l_1l_2}^2}}v+\mu_{Y_{\mathrm{HI}_2}}\right)|J|\,\mathrm{d}u\mathrm{d}v \\ &= \int_{-\frac{\sqrt{1-\rho_{l_1l_2}^2}\mu_{Y_{\mathrm{HI}_2}}}{\sqrt{2}\sigma_{Y_{\mathrm{HI}_2}}}}^{+\infty}\int_{-\frac{\mu_{Y_{\mathrm{HI}_1}}}{\sqrt{2}\sigma_{Y_{\mathrm{HI}_1}}}-\frac{\rho_{l_1l_2}v}{\sqrt{1-\rho_{l_1l_2}^2}}}^{+\infty}\frac{1}{\pi\left(1-\rho_{l_1l_2}^2\right)}\exp\left\{-\frac{u^2+v^2}{1-\rho_{l_1l_2}^2}\right\} \\ &\times\left(\sqrt{2}\sigma_{Y_{\mathrm{HI}_1}}u+\frac{\sqrt{2}\rho_{l_1l_2}\sigma_{Y_{\mathrm{HI}_1}}}{\sqrt{1-\rho_{l_1l_2}^2}}v+\mu_{Y_{\mathrm{HI}_1}}\right)\left(\frac{\sqrt{2}\rho_{l_1l_2}\sigma_{Y_{\mathrm{HI}_2}}}{\sqrt{1-\rho_{l_1l_2}^2}}v+\mu_{Y_{\mathrm{HI}_2}}\right)\mathrm{d}u\mathrm{d}v \end{aligned} \tag{C-5}$$

The above equation can be further transformed into the following univariate integral:

$$E\left(Y_{\mathrm{ReLU}l_1}Y_{\mathrm{ReLU}l_2}\right) = \int_{-\frac{\sqrt{1-\rho_{l_1l_2}^2}\mu_{Y_{\mathrm{HI}_2}}}{\sqrt{2}\sigma_{Y_{\mathrm{HI}_2}}}}^{+\infty}\frac{\frac{\sqrt{2}\sigma_{Y_{\mathrm{HI}_2}}v}{\sqrt{1-\rho_{l_1l_2}^2}}+\mu_{Y_{\mathrm{HI}_2}}}{2\pi\left(1-\rho_{l_1l_2}^2\right)}\exp\left\{-\frac{v^2}{1-\rho_{l_1l_2}^2}\right\}\left(\sqrt{2}\sigma_{Y_{\mathrm{HI}_1}}Q_1-\sqrt{\pi}\sqrt{1-\rho_{l_1l_2}^2}\mu_{Y_{\mathrm{HI}_1}}Q_2\right)\mathrm{d}v \tag{C-6}$$

in which

$$Q_1 = \left(1-\rho_{l_1l_2}^2\right)\exp\left\{-\frac{\left(2\rho_{l_1l_2}\sigma_{Y_{\mathrm{HI}_1}}v+\sqrt{2-2\rho_{l_1l_2}^2}\mu_{Y_{\mathrm{HI}_1}}\right)^2}{4\left(1-\rho_{l_1l_2}^2\right)^2\sigma_{Y_{\mathrm{HI}_1}}^2}\right\}+\sqrt{\pi}\rho_{l_1l_2}v-\sqrt{\pi}\rho_{l_1l_2}v\mathrm{Erf}\left[-\frac{2\rho_{l_1l_2}\sigma_{Y_{\mathrm{HI}_1}}v+\sqrt{2-2\rho_{l_1l_2}^2}\mu_{Y_{\mathrm{HI}_1}}}{2\left(1-\rho_{l_1l_2}^2\right)\sigma_{Y_{\mathrm{HI}_1}}}\right] \tag{C-7}$$

$$Q_2 = \mathrm{Erf}\left[-\frac{2\rho_{l_1l_2}\sigma_{Y_{\mathrm{HI}_1}}v+\sqrt{2-2\rho_{l_1l_2}^2}\mu_{Y_{\mathrm{HI}_1}}}{2\left(1-\rho_{l_1l_2}^2\right)\sigma_{Y_{\mathrm{HI}_1}}}\right]-1 \tag{C-8}$$

where $\mathrm{Erf}[\cdot]$ represents the Gaussian error function.

References

[1] Coleman H W and Steele W G 2018 *Experimentation, Validation, and Uncertainty Analysis for Engineers* (Wiley)

[2] Wang C and Matthies H G 2020 A modified parallelepiped model for non-probabilistic uncertainty quantification and propagation analysis *Comput. Methods Appl. Mech. Eng.* **369** 113209

[3] Shi Y, Lu Z, Huang Z, Xu L and He R 2020 Advanced solution strategies for time-dependent reliability based design optimization *Comput. Methods Appl. Mech. Eng.* **364** 112916

[4] Mohammadi S and Cremaschi S 2022 Efficiency of uncertainty propagation methods for moment estimation of uncertain model outputs *Comput. Chem. Eng.* **166** 107954

[5] Chen Y L, Shi Y, Huang H Z, Sun D and Beer M 2023 Uncertainty analysis of structural output with closed-form expression based on surrogate model *Probab. Eng. Mech.* **73** 103482

[6] Shi Y, Lu Z, Chen S and Xu L 2018 A reliability analysis method based on analytical expressions of the first four moments of the surrogate model of the performance function *Mech. Syst. Signal Process.* **111** 47–67

[7] Meng X, Liu J, Cao L, Yu Z and Yang D 2020 A general frame for uncertainty propagation under multimodally distributed random variables *Comput. Methods Appl. Mech. Eng.* **367** 113109

[8] Liu H B, Jiang C, Jia X Y, Long X Y, Zhang Z and Guan F J 2018 A new uncertainty propagation method for problems with parameterized probability-boxes *Reliab. Eng. Syst. Saf.* **172** 64–73

[9] Melchers R E and Beck A T 2018 *Structural Reliability Analysis and Prediction* (Wiley)

[10] Shi Y, Lu Z, He R, Zhou Y and Chen S 2020 A novel learning function based on Kriging for reliability analysis *Reliab. Eng. Syst. Saf.* **198** 106857

[11] McKay M D, Beckman R J and Conover W J 2000 A comparison of three methods for selecting values of input variables in the analysis of output from a computer code *Technometrics* **42** 55–61

[12] Sobol' I M 1967 On the distribution of points in a cube and the approximate evaluation of integrals *Zh. Vychisl. Mat. Mat. Fiz.* **7** 784–802

[13] Halton J H 1960 On the efficiency of certain quasi-random sequences of points in evaluating multi-dimensional integrals *Numer. Math.* **2** 84–90

[14] Evans D H 1972 An application of numerical integration techniques to statistical tolerancing, III-general distributions *Technometrics* **14** 23–35
[15] Rahman S and Xu H 2004 A univariate dimension-reduction method for multi-dimensional integration in stochastic mechanics *Probab. Eng. Mech.* **19** 393–408
[16] Smolyak S A 1963 Quadrature and interpolation formulas for tensor products of certain classes of functions *Proc. Doklady Akademii Nauk* (Russian Academy of Sciences) vol 148 pp 1042–5
[17] O'Hagan A 2013 Polynomial chaos: a tutorial and critique from a statistician's perspective *SIAM/ASA J. Uncertain. Quantif.* **20** 1–20
[18] Wang C and Matthies H G 2020 A comparative study of two interval-random models for hybrid uncertainty propagation analysis *Mech. Syst. Signal Process.* **136** 106531
[19] Wei P, Zhang X and Beer M 2020 Adaptive experiment design for probabilistic integration *Comput. Methods Appl. Mech. Eng.* **365** 113035
[20] Sudret B, Marelli S and Wiart J 2017 Surrogate models for uncertainty quantification: an overview *2017 11th European Conf. on Antennas and Propagation (EUCAP)* (IEEE) pp 793–97
[21] Abramowitz M, Stegun I A and Romer R H 1988 Handbook of mathematical functions with formulas, graphs, and mathematical tables *Am. J. Phys.* **56** 958
[22] He J, Gao S and Gong J 2014 A sparse grid stochastic collocation method for structural reliability analysis *Struct. Saf.* **51** 29–34
[23] Lophaven S N, Nielsen H B and Søndergaard J 2002 *DACE: A Matlab Kriging Toolbox* (IMM, Informatics and Mathematical Modelling, The Technical University of Denmark)
[24] Williams C K I and Rasmussen C E 2006 *Gaussian Processes for Machine Learning* (MIT Press)
[25] Keshtegar B, Seghier M E A B, Zio E, Correia J A F O, Zhu S-P and Trung N-T 2021 Novel efficient method for structural reliability analysis using hybrid nonlinear conjugate map-based support vector regression *Comput. Methods Appl. Mech. Eng.* **381** 113818
[26] Cao L, Liu J, Jiang C and Liu G 2022 Optimal sparse polynomial chaos expansion for arbitrary probability distribution and its application on global sensitivity analysis *Comput. Methods Appl. Mech. Eng.* **399** 115368
[27] Luo C, Keshtegar B, Zhu S P, Taylan O and Niu X-P 2022 Hybrid enhanced Monte Carlo simulation coupled with advanced machine learning approach for accurate and efficient structural reliability analysis *Comput. Methods Appl. Mech. Eng.* **388** 114218
[28] Peherstorfer B, Cui T, Marzouk Y and Willcox K 2016 Multifidelity importance sampling *Comput. Methods Appl. Mech. Eng.* **300** 490–509
[29] Pradlwarter H J, Schueller G I, Koutsourelakis P S and Charmpis D C 2007 Application of line sampling simulation method to reliability benchmark problems *Struct. Saf.* **29** 208–21
[30] Pearson K IX. 1916 Mathematical contributions to the theory of evolution.-XIX. Second supplement to a memoir on skew variation *Phil. Trans. R. Soc.* A **216** 429–57
[31] Slifker J F and Shapiro S S 1980 The Johnson system: selection and parameter estimation *Technometrics* **22** 239–46
[32] Low Y M 2013 A new distribution for fitting four moments and its applications to reliability analysis *Struct. Saf.* **42** 12–25
[33] Crombecq K, Gorissen D, Deschrijver D and Dhaene T 2011 A novel hybrid sequential design strategy for global surrogate modeling of computer experiments *SIAM J. Sci. Comput.* **33** 1948–74
[34] Kaminsky A L, Wang Y and Pant K 2021 An efficient batch K-fold cross-validation voronoi adaptive sampling technique for global surrogate modeling *J. Mech. Des.* **143** 011706
[35] Tripathy R K and Bilionis I 2018 Deep UQ: learning deep neural network surrogate models for high dimensional uncertainty quantification *J. Comput. Phys.* **375** 565–88
[36] Liu J F, Jiang C and Zheng J 2022 Uncertainty propagation method for high-dimensional black-box problems via Bayesian deep neural network *Struct. Multidiscipl. Optim.* **65** 83
[37] Liu J, Jiang C, Liu H and Li G 2023 A time variant uncertainty propagation method for high-dimensional dynamic structural system via K–L expansion and Bayesian deep neural network *Phil. Trans. R. Soc.* A **381** 20220388
[38] Shi Y, Chai R and Beer M 2024 Novel gradient-enhanced Bayesian neural networks for uncertainty propagation *Comput. Methods Appl. Mech. Eng.* **429** 117188
[39] Wang C, Qiang X, Xu M and Wu T 2022 Recent advances in surrogate modeling methods for uncertainty quantification and propagation *Symmetry* **14** 1219
[40] Xiao X, Li Q and Wang Z 2023 A robust method for reliability updating with equality information using sequential adaptive importance sampling *Comput. Methods Appl. Mech. Eng.* **410** 116028
[41] Tabandeh A, Jia G and Gardoni P 2022 A review and assessment of importance sampling methods for reliability analysis *Struct. Saf.* **97** 102216
[42] Zhao Y G and Ono T 2001 Moment methods for structural reliability *Struct. Saf.* **23** 47–75
[43] Lu H, Cao S, Zhu Z and Zhang Y 2020 An improved high order moment-based saddlepoint approximation method for reliability analysis *Appl. Math. Modelling* **82** 836–47
[44] Hong L, Li H and Fu J 2022 A novel surrogate-model based active learning method for structural reliability analysis *Comput. Methods Appl. Mech. Eng.* **394** 114835
[45] Shi Y, Lu Z, Xu L and Chen S 2019 An adaptive multiple-Kriging-surrogate method for time-dependent reliability analysis *Appl. Math. Modelling* **70** 545–71
[46] Au S K, Ching J and Beck J L 2007 Application of subset simulation methods to reliability benchmark problems *Struct. Saf.* **29** 183–93
[47] de Angelis M, Patelli E and Beer M 2015 Advanced line sampling for efficient robust reliability analysis *Struct. Saf.* **52** 170–82
[48] Bichon B J, Eldred M S, Swiler L P, Mahadevan S and McFarland J M 2008 Efficient global reliability analysis for nonlinear implicit performance functions *AIAA J.* **46** 2459–68
[49] Echard B, Gayton N and Lemaire M 2011 AK-MCS: an active learning reliability method combining Kriging and Monte Carlo simulation *Struct. Saf.* **33** 145–54
[50] Lv Z, Lu Z and Wang P 2015 A new learning function for Kriging and its applications to solve reliability problems in engineering *Comput. Math. Appl.* **70** 1182–97
[51] Teixeira R, Nogal M and O'Connor A 2021 Adaptive approaches in metamodel-based reliability analysis: a review *Struct. Saf.* **89** 102019
[52] Afshari S S, Enayatollahi F, Xu X and Liang X 2022 Machine learning-based methods in structural reliability analysis: a review *Reliab. Eng. Syst. Saf.* **219** 108223
[53] Giovanis D G, Papaioannou I, Straub D and Papadopoulos V 2017 Bayesian updating with subset simulation using artificial neural networks *Comput. Methods Appl. Mech. Eng.* **319** 124–45
[54] Yegnanarayana B 2009 *Artificial Neural Networks* (PHI Learning Pvt. Ltd)

[55] Ji W, Ren Z and Law C K 2019 Uncertainty propagation in deep neural network using active subspace (arXiv:1903.03989)
[56] Astudillo R F and da Silva Neto J P 2011 Propagation of uncertainty through multilayer perceptrons for robust automatic speech recognition *12th Annual Conf. Int. Speech Communication Association* pp 461–64
[57] Bibi A, Alfadly M and Ghanem B 2018 Analytic expressions for probabilistic moments of pl-dnn with gaussian input *Proc. IEEE Conf. on Computer Vision and Pattern Recognition* pp 9099–107
[58] Beiu V, Peperstraete J A, Vandewalle J and Lauwereins R 1994 *VLSI Complexity Reduction by Piece-wise Approximation of the Sigmoid Function* (ESANN)
[59] Julier S J and Uhlmann J K 1997 New extension of the Kalman filter to nonlinear systems *Signal Processing, Sensor Fusion, and Target Recognition VI* pp 182–93
[60] Abdelaziz A H, Watanabe S, Hershey J R, Vincent E and Kolossa D 2015 Uncertainty propagation through deep neural networks *Interspeech 2015*
[61] Rosenblatt M 1952 Remarks on a multivariate transformation *Ann. Math. Stat.* **23** 470–2
[62] Glorot X, Bordes A and Bengio Y 2011 Deep sparse rectifier neural networks *Proc. 14th Int. Conf. on Artificial Intelligence and Statistics. JMLR Workshop and Conf. Proc.* 315–23
[63] Gu J *et al* 2018 Recent advances in convolutional neural networks *Pattern Recognit.* **77** 354–77
[64] Kingma D P and Ba J 2014 Adam: a method for stochastic optimization (arXiv:1412.6980)
[65] Fauriat W and Gayton N 2014 AK-SYS: an adaptation of the AK-MCS method for system reliability *Reliab. Eng. Syst. Saf.* **123** 137–44
[66] Shi Y and Beer M 2024 Deep learning-driven interval uncertainty propagation for aeronautical structures *Chin. J. Aeronaut.* **37** 71–86
[67] Dubey S R, Singh S K and Chaudhuri B B 2022 Activation functions in deep learning: a comprehensive survey and benchmark *Neurocomputing* **503** 92–108

Yan Shi received the B.E. degree and PhD degree in School of Aeronautics from Northwestern Polytechnical University, Xi'an, China. He is currently an Alexander von Humboldt Fellow at Institute for Risk and Reliability, Leibniz Universität Hannover. His research interests include structural/system/network reliability analysis, sensitivity analysis, design optimization, and machine learning techniques.

Lizhi Niu received the B.S. degree and M.S degree from School of Mathematics and Statistics from Northwestern Polytechnical University, Xi'an, China, and he is a dual PhD candidate in School of Mathematics and Statistics from Northwestern Polytechnical University, Xi'an, China, as well as department of Engineering from University of Palermo, Palermo, Italy. His research interests include probability response of stochastic dynamic system, stochastic reliability analysis, integral transform and fractional calculus.

Michael Beer received the M.S. degree and PhD degree in Civil Engineering from Technische Universität Dresden (TU Dresden), Dresden, Germany. He is a Full Professor and Head of the Institute for Risk and Reliability at Leibniz Universität Hannover. He is also part time Professor of the Institute for Risk and Uncertainty at University of Liverpool, and Guest Professor of the International Joint Research Center for Resilient Infrastructure & International Joint Research Center for Engineering Reliability and Stochastic Mechanics at Tongji University. He mainly focuses on efficient stochastic analysis of engineering systems and structures, including response characterization, reliability analysis, sensitivity analysis, and robust and reliability-based design optimization.

079